Plant Physiology®

Plant Physiology, 2025, **198**, kiaf284
https://doi.org/10.1093/plphys/kiaf284
Advance access publication 2 July 2025
Research Article

The susceptibility factor *Resistance To Phytophthora parasitica 1* negatively regulates Arabidopsis immunity by interacting with the cytochrome P450 protein CYP71B3

Yushu Wei,[†] Deqian Zong,[†] Yaling Tang, Lehui Kong, Xianxian Gao, Xiaoxue Wang, Yingqi Zhang, Yang Yang, Xiaoyu Qiang,[*] Weixing Shan[*]

State Key Laboratory for Crop Stress Resistance and High-Efficiency Production and College of Agronomy, Northwest A&F University, Yangling 712100, China
[*]Author for correspondence: qiangxiaoyu@nwafu.edu.cn (X.Q.), wxshan@nwafu.edu.cn (W.S.)
[†]These authors contributed equally to this work.
The author responsible for distribution of materials integral to the findings presented in this article in accordance with the policy described in the Instructions for Authors (https://academic.oup.com/plphys/pages/General-Instructions) is Weixing Shan (wxshan@nwafu.edu.cn).

Abstract

Oomycetes, particularly *Phytophthora* species, cause destructive plant diseases that severely threaten sustainable crop production. Due to the loss of genotype-specific disease resistance, it is important to identify and understand immune factors that mediate plant susceptibility. Loss-of-function of the susceptibility factor resistance to *Phytophthora parasitica* 1 (RTP1) leads to broad-spectrum disease resistance in *Arabidopsis thaliana* (*A. thaliana (L.) Heynh.*). Through RNA-seq analysis, we determined that *CYP71B3*, encoding an uncharacterized P450 enzyme, is significantly upregulated in *rtp1* mutant plants infected with *P. parasitica*. Loss-of-function of CYP71B3 led to abolished pathogen-associated molecular pattern (PAMP)–triggered oxidative burst and rendered *Arabidopsis* more susceptible to diverse pathogens, including the oomycete *P. parasitica* and bacterial *Pseudomonas syringae*. Conversely, overexpression of *CYP71B3* enhanced plant resistance and PAMP-triggered oxidative burst. CYP71B3 localized in the endoplasmic reticulum and was destabilized by interacting with RTP1 via the I-38 residue, which is essential for its immune function and P450 enzyme activity. The expression of *CYP71B3* was regulated by transcription factor bZIP60, which is required for *rtp1*-mediated resistance to *P. parasitica*. Our studies indicate that RTP1 mediates plant susceptibility by destabilizing the downstream positive immune factor CYP71B3.

Introduction

To resist attack from a plethora of pathogens, plants activate a series of defense responses, including pattern-triggered immunity (PTI) and effector-triggered immunity (ETI). PTI is often accompanied by reactive oxygen species (ROS) production (Wojtaszek 1997), induction of downstream immunity-related genes, and phytoalexin biosynthesis. ETI is often accompanied by the hypersensitive response (Jones and Dangl 2006; Boller and He 2009; Dodds and Rathjen 2010). ETI and PTI can cooperate via the production of ROS to circumvent pathogen attack (Yuan et al. 2021).

Cytochrome P450 (CYP) enzymes widely exist in most species that are particularly distributed among plants and function in the catalysis of diverse secondary metabolites. Typically, eukaryotic CYP450 enzymes are endoplasmic reticulum (ER) membrane-bound proteins in which the N-terminal hydrophobic helices are anchored on the ER membrane (Neve and Ingelman-Sundberg 2010). In *Arabidopsis*, many *CYP* family genes, particularly the *CYP71* family genes, play an important role in plant resistance to multiple pathogens (Kliebenstein et al. 2005; Glawischnig 2006; Schlaeppi et al. 2010). Among these genes, *CYP71A12*, *CYP71A13*, *CYP79B2*, *CYP79B3*, and *CYP71B15* (PHYTOALEXIN DEFICIENT 3 [*PAD3*]) have been identified to be crucial in the camalexin biosynthesis (Yoshihiro et al. 2003; Zhao et al. 2003; Müller et al. 2015). And the promoters of these genes contain the TTGACC W-box element, which is required for binding to and their regulation by the WRKY33 transcription factor (TF) (Eulgem et al. 2000; Petersen et al. 2008; Qiu et al. 2008; Mao et al. 2011; Birkenbihl et al. 2017). Further studies revealed that calcium protein kinase (CPK) 5/CPK6 and mitogen-activated protein kinase (MPK) 3/MPK6 could phosphorylate and activate WRKY33, which consequently regulates the expression of these *CYP* genes to regulate plant immunity (Yang *et al.* 2020a; Zhou et al. 2020). In rice, the basic region-leucine zipper (bZIP) TF AVRPIZ-T-INTERACTING PROTEIN 5 was reported to negatively regulate plant cell death and blast resistance via directly targeting the cytochrome P450 gene *CYP72A1* and inhibits its expression. Consequently, the ROS production and defense compounds accumulation were limited (Zhang et al. 2022).

Oomycetes, particularly *Phytophthora* species, cause most devastating crop diseases, such as potato late blight and tobacco black shank, which severely reduce crop yields worldwide. Given the prevalence of variability in pathogen virulence and loss-of-function of genotype-specific resistance genes in the host plant (Fry 2008; Panstruga and Dodds 2009), it is urgent to identify novel immune regulators that have great potential to confer plant durable disease resistance (Schie and Takken 2014). *Phytophthora parasitica*, a model oomycete, is a hemibiotrophic pathogen that infects a broad range of plants and causes extensive damage to crop production (Kamoun et al. 2015). By employing the *Arabidopsis thaliana thaliana–P. parasitica* model pathosystem (Meng et al. 2014; Wang et al. 2011), our previous studies demonstrated more rapid colonization of *P. parasitica* in *Arabidopsis* roots

Received April 6, 2025. Accepted May 22, 2025.

rather than leaves, in which the pathogen could penetrate at 3 h past inoculation (hpi), and form appressoria at 6 hpi and develop haustoria-like structure at 12 hpi, representing the biotrophic infection stages (Wang et al. 2011; Meng et al. 2015). Based on this model pathosystem, several negative regulators of plant immunity have been identified (Li et al. 2019, 2022; Lu et al. 2020; Pan et al. 2016; Yang *et al.* 2020b, 2022). Among them, the susceptibility factor resistance to *P. parasitica* 1 (*RTP1*) encodes an ER membrane-localized protein and negatively regulates *Arabidopsis* resistance to multiple biotrophic pathogens, including bacterial *Pseudomonas syringae*, possibly by regulating plant cell death, ROS production, and *PR1* expression during the early infection stage (Pan et al. 2016).

Further studies demonstrate that RTP1 negatively regulates *Arabidopsis* resistance to *P. parasitica* by modulating ER membrane-associated TFs bZIP60 and bZIP28, 2 key regulators of the ER stress response (Qiang et al. 2021). This prompted us to further explore the downstream immune-regulatory factors in RTP1-mediated immune pathway.

In this study, we performed transcriptome sequencing of *Arabidopsis* wild-type (WT) Columbia-0 (Col-0) and *rtp1* mutant plants during the early colonization of *P. parasitica* and identified *CYP71B3*, encoding an uncharacterized cytochrome P450 protein, was differentially expressed in *rtp1* mutants compared with the WT. Further pathogenicity assays demonstrate that CYP71B3 contributes to alleviate RTP1-mediated susceptibility to *P. parasitica* and plays a positive role in *Arabidopsis* resistance against a broad spectrum of pathogens and pathogen-associated molecular pattern (PAMP)–triggered oxidative burst. Furthermore, we show that the ER-localized CYP71B3 interacts with and is destabilized by RTP1 via its I-38 residue, an essential site for the immune function and P450 enzyme activity of CYP71B3. We also found that the bZIP60 TF, whose activation was modulated by RTP1, could bind to the promoter of *CYP71B3* to regulate its expression. Together, our studies identify CYP71B3 as a positive immune factor, which could interact with and be destabilized via its I-38 residue by the susceptibility factor RTP1. These also help expand understanding of the regulatory mechanism of plant susceptibility mediated by RTP1.

Results

CYP71B3 is upregulated in the *rtp1* mutant during early infection by *P. parasitica*

To identify immune regulators with a crucial function in *rtp1*-mediated resistance, we sequenced the transcriptome of *Arabidopsis* roots from WT Col-0 and the *rtp1* mutant infected by *P. parasitica* at 3 and 6 hpi, representing the early biotrophic infection stages. The analysis detected 252 and 1161 genes that were upregulated in the *rtp1* mutant when compared with the WT at 3 and 6 hpi, respectively ($\log_2$ [fold change] ≥ 2; *P*-value ≤ 0.05) (Supplementary Fig. S1A). Among them, 102 genes were upregulated at both 3 and 6 hpi (Supplementary Fig. S1B). Further Kyoto Encyclopedia of Genes and Genomes (KEGG) pathway analyses revealed that most of the differentially expressed genes (DEGs) in *rtp1* mutants were associated with phenylpropanoid biosynthesis and protein processing in ER at 3 dpi, and associated with plant–pathogen interaction, oxidative phosphorylation, and phenylpropanoid biosynthesis at 6 hpi (Fig. 1A). Notably, further expression heatmap analysis on DEGs enriched in the phenylpropanoid biosynthesis pathway indicated that many *CYP71* family genes induced upon infection by *P. parasitica* (fragments per kilo base per million mapped reads [FPKM] > 0) (Supplementary Table S1), were generally upregulated in the *rtp1* mutant as compared to WT, at the early colonization stage (Fig. 1B). To further confirm the differential regulation of these *CYP71* family genes in the *rtp1* plants, the expression of the most significantly upregulated genes in infected *rtp1* plants at both 3 and 6 hpi ($\log_2$[fold change] > 1; *P*-value < 0.05), including *CYP71B3*, *CYP71B21*, *CYP71B22*, *CYP71B20*, *CYP71A12*, and *CYP71A13* as well as *CYP71B15* (*PAD3*), was examined by reverse-transcription quantitative PCR (RT-qPCR) (Fig. 1C; Supplementary Table S1). The results showed that except for the downregulation of *CYP71B21* (Supplementary Fig. S2), expression levels of *CYP71B3*, *CYP71B22*, *CYP71A13*, and *PAD3* were significantly elevated in *P. parasitica*-infected *rtp1* plants from 3 to 6 hpi, and their expression was much strongly induced at 12 hpi in *rtp1* mutants when compared with WT (Fig. 1C). The expression of *CYP71A12* was highly induced in *rtp1* mutants at 12 hpi as shown previously (Qiang et al. 2021). Collectively, these data suggest that the expression of multiple *CYP71* family genes, including *CYP71B3*, is upregulated in *P. parasitica*-infected *rtp1* mutant plants.

CYP71B3 contributes to alleviate RTP1-mediated susceptibility to *P. parasitica*

Based on those results, we hypothesized that some *CYP71* family genes might be involved in resistance in *rtp1* plants. Among the notably upregulated genes in the *rtp1* mutant during early colonization by *P. parasitica* (Fig. 1C), several genes were known to be involved in camalexin biosynthesis, which play a role in plant immunity, including *CYP71A12*, *CYP71A13*, and *PAD3* (Yoshihiro et al. 2003; Müller et al. 2015), whereas *CYP71B3*, *CYP71B20*, and *CYP71B22* were uncharacterized P450 genes. To investigate their immune function, we employed *Agrobacterium tumefaciens*–mediated transient gene expression assay in leaves of *Nicotiana benthamiana* and performed infection assay. The results indicated that overexpression (OE) of CYP71B3, but not CYP71B20 and CYP71B22, could significantly enhance plant resistance against *P. parasitica* (Supplementary Fig. S3).

As the transcriptomic analyses predicted that *CYP71B3* was induced by various biotic and abiotic stresses (Supplementary Fig. S4, C and D; Kreps et al. 2002; Ascencio-Ibáñez et al. 2008), we therefore focused on *CYP71B3* and investigated if its OE had an effect on RTP1-mediated susceptibility. We coinfiltrated the constructs of 35S::*CYP71B3* and 35S::*RTP1* as well as 35S::*RTP1* and 35S::*GFP* as control into *N. benthamiana* leaves prior to inoculation with *P. parasitica*. Significantly smaller infection lesions were observed in the leaf region infiltrated with 35S::*CYP71B3* and 35S::*RTP1* compared with control (Fig. 2, A and B; Supplementary Fig. S5A). The proteins expression and integrity were confirmed by western blot (Fig. 2C). These results suggest that CYP71B3 might contribute to alleviate RTP1-mediated susceptibility to *P. parasitica*.

To further investigate the role of CYP71B3 in *rtp1*-mediated resistance to *P. parasitica*, we generated *rtp1cyp71b3* double mutant by crossing *rtp1* with *cyp71b3* (Supplementary Fig. S6, A, C, and D). The detached leaves of 6-wk-old mutant plants of *rtp1*, *cyp71b3*, and *rtp1cyp71b3* as well as WT Col-0 were inoculated with *P. parasitica* zoospores. At 72 hpi, both *cyp71b3* and *rtp1cyp71b3* mutants were significantly more susceptible, with larger water-soaked lesions and more pathogen biomass than *rtp1* and WT (Fig. 2, D and E; Supplementary Fig. S5B). These results indicate that CYP71B3 plays a role in *rtp1*-mediated plant resistance to *P. parasitica* and might function downstream of RTP1.

CYP71B3 plays a positive role in plant resistance against oomycete *P. parasitica* and bacterial Pst DC3000

In order to further explore the immune function of CYP71B3, we performed genetic complementation (CM) experiments in the *cyp71b3* background and *CYP71B3* OE experiments in Col-0

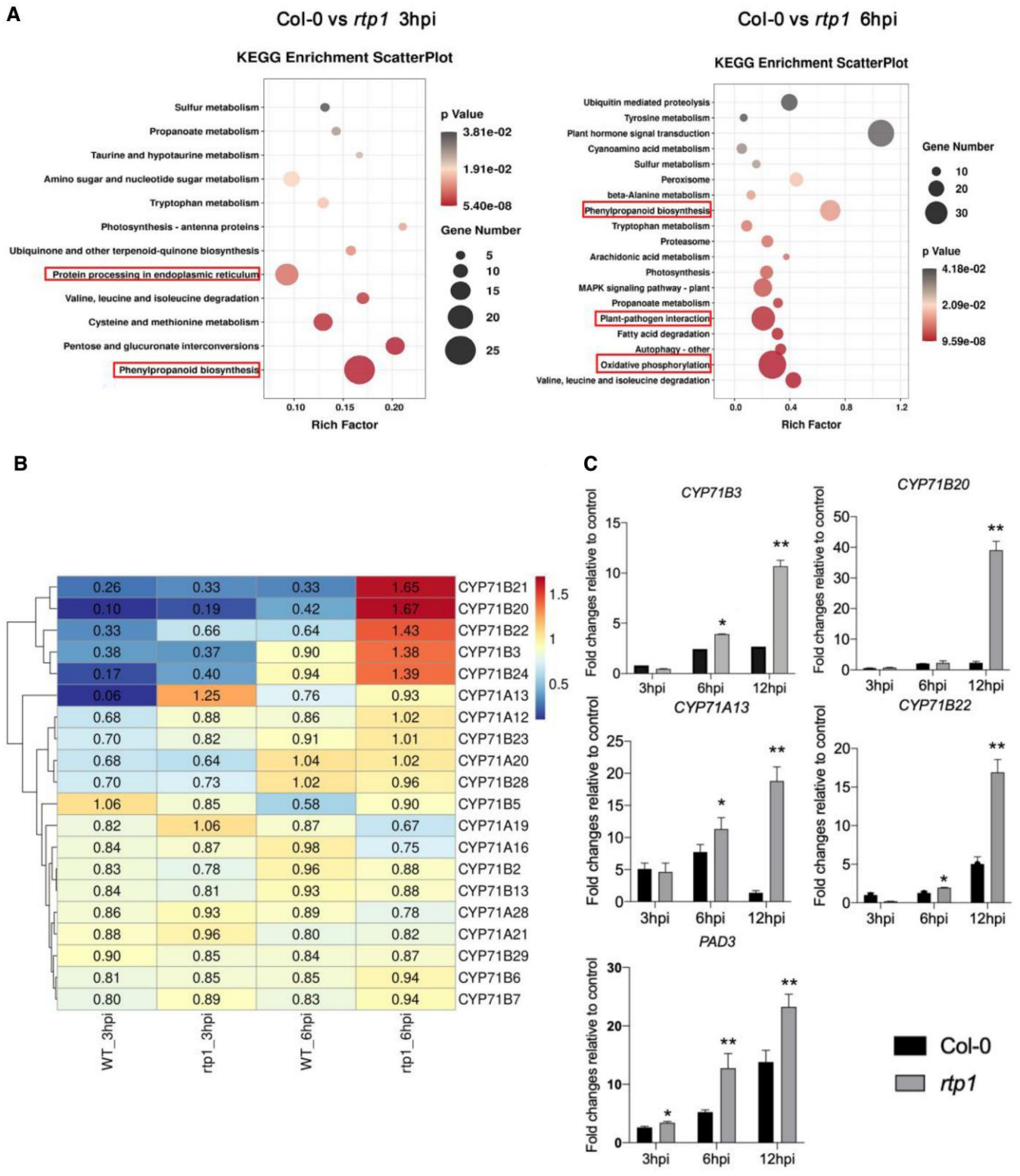

Figure 1. Many *CYP71* family genes are upregulated in *Arabidopsis rtp1* roots during early infection by *P. parasitica*. **A)** The KEGG bubble plot of upregulated genes in *rtp1* at 3 and 6 hpi. The ordinate represents the enriched items of KEGG analysis, and different colors represent the *P*-value. From red to gray represents increased significant difference (*P*-value), and the size of circle represents the number of genes enriched to the same KEGG item. **B)** Visualization of gene expression levels (log_2FPKM) of upregulated *CYP71* family genes in *rtp1* mutant roots at 3 and 6 hpi, respectively. **C)** The expression levels of major upregulated genes including *CYP71B3*, *CYP71B20*, *CYP71B22*, *CYP71A13*, and *PAD3* were evaluated by RT-qPCR. The ordinate was the fold change of gene expression, and the abscissa was the time points postinoculation. Data presented show means of 3 independent experiments ± SD. Asterisks indicate significant differences at $^*P < 0.05$, $^{**}P < 0.01$, and $^{***}P < 0.001$ analyzed by Student's *t*-test. FPKM, fragments per kilobase of transcript per million mapped reads.

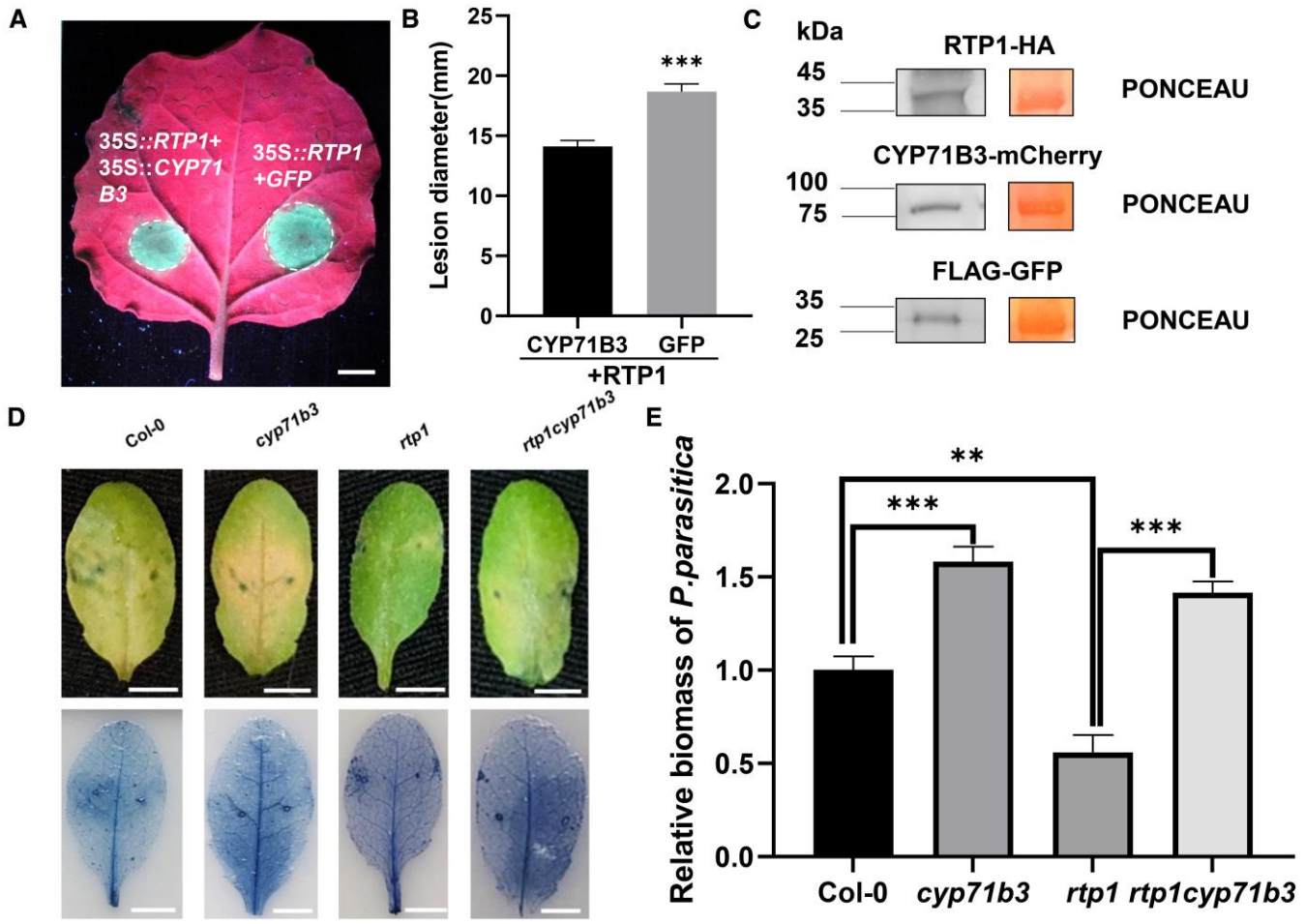

Figure 2. CYP71B3 contributes to alleviate RTP1-mediated plant susceptibility to *P. parasitica*. **A** and **B)** RTP1-HA with either CYP71B3-mCherry or FLAG-GFP were transiently coexpressed in *N. benthamiana* leaves prior to inoculation with *P. parasitica* zoospores. UV exposure and measurement of lesions diameter were performed at 48 hpi). Scale bar, 1 cm. At least 20 leaves were used for each test. Error bars represent SD, and asterisks indicate statistical significance based on a *t*-test (***$P < 0.001$). Similar results were obtained for at least 3 individual experiments. See also Supplementary Fig. S5A. **C)** CYP71B3-mCherry, RTP1-HA, and FLAG-GFP were transiently expressed in *N. benthamiana* leaves through infiltration with an *A. tumefaciens* cell suspension ($OD_{600} = 0.4$), and immunoblot analysis was performed using indicated antibody. **D)** Detached leaves of 4-wk-old *rtp1cyp71b3* and *cyp71b3* plants showed susceptibility to infection by *P. parasitica* zoospores, whereas *rtp1* showed resistance at 3 dpi, relative to WT Col-0. Scale bar, 0.5 cm. At least 3 independent experiments were performed, and 20 plants per line were analyzed. See also Supplementary Fig. S5B. **E)** Quantification of *P. parasitica* biomass in infected leaves of WT Col-0, mutants *cyp71b3*, *rtp1*, and *rtp1cyp71b3* at 72 hpi. The biomass of *P. parasitica* in all lines was normalized with that in WT Col-0 (set to 1). Sample size is 3. Bars represent SD. Asterisks denote significance analyzed by Student's *t*-test (*$P < 0.05$; **$P < 0.01$; ***$P < 0.001$).

(WT background). The transgenic plants showed no obvious changes in growth or morphology as compared with WT plants (Supplementary Fig. S6A). The transcript levels of *CYP71B3* in both CYP71B3-CM and CYP71B3-OE lines were confirmed by RT-qPCR (Supplementary Fig. S6B). Subsequently, the confirmed homozygous transgenic plants were used to analyze the immune function of CYP71B3 in response to *P. parasitica* infection. Pathogenicity assays showed that *P. parasitica* colonized more severely in leaves of *cyp71b3* mutants, as indicated by larger infection lesions and significantly higher pathogen biomass than that in WT Col-0 (Fig. 3, A and B; Supplementary Fig. S7A). Root-dip inoculation with *P. parasitica* zoospores also showed higher pathogen biomass in *cyp71b3* mutant roots (Fig. 3, C and D; Supplementary Fig. S7C). By contrast, much smaller infection lesions were observed, and lower pathogen biomass was quantified in leaves of both CYP71B3-OE and CYP71B3-CM lines relative to WT and *cyp71b3* mutants (Fig. 3, A and B). This implied that OE of *CYP71B3* increased plant resistance to *P. parasitica* and reversed the susceptible phenotype of *cyp71b3*. These results support the notion that CYP71B3 might function as a positive regulator in plant resistance against *P. parasitica* infection.

Given that the susceptibility factor RTP1 regulates plant resistance against a variety of biotrophic pathogens, we next investigated the function of CYP71B3 in resistance to the biotrophic bacterial pathogen *Pst* DC3000 (*P. syringae*). The leaves of *cyp71b3* mutant, CYP71B3-CM and CYP71B3-OE lines as well as Col-0 were infiltrated with *Pst* DC3000 at the concentration of 4×10^5 CFU mL^{-1}. At 3 dpi, *cyp71b3* plants displayed more susceptible, with increased titer of bacteria relative to WT Col-0. By contrast, significantly reduced bacterial colonization was detected in CYP71B3-OE plants compared with WT Col-0 (Fig. 3F).

CYP71B3 positively affects PAMP-triggered ROS production in plant

As *RTP1* negatively regulates *P. parasitica* resistance by affecting the ROS production (Pan et al. 2016), we investigated whether *CYP71B3* participates in the regulation of ROS production. The ROS burst response induced by the immune elicitor flg22 (Gómez-Gómez and

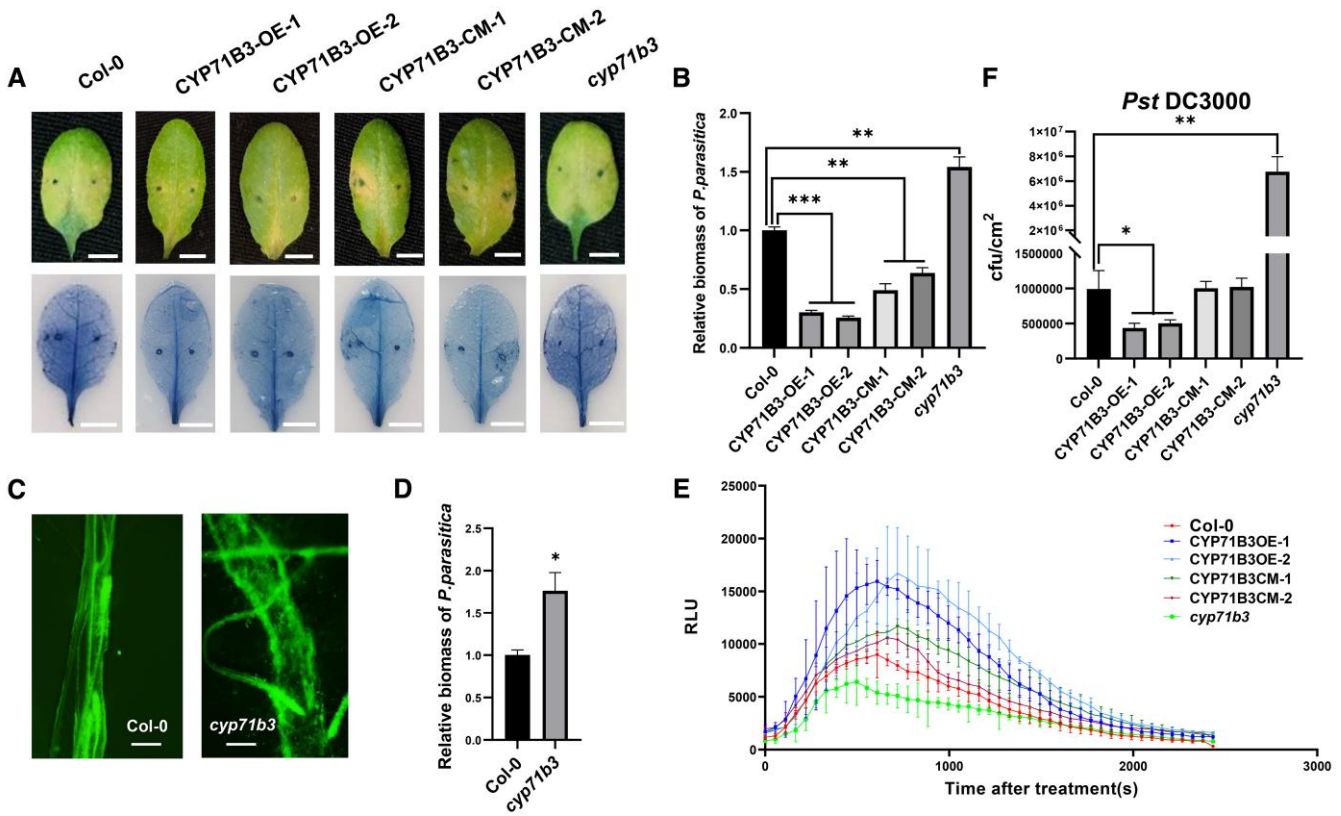

Figure 3. CYP71B3 plays a positive role in *Arabidopsis* resistance to multiple pathogens and PAMP-triggered oxidative burst. **A)** Detached leaves of 4-wk-old *cyp71b3*, *CYP71B3* OE (OE-1 and OE-2), *CYP71B3* CM (CM-1 and CM-2), and WT Col-0 plants were inoculated with *P. parasitica* zoospores. The water-soaked lesions with trypan blue staining were photographed at 3 d past inoculation (dpi). Scale bar, 0.5 cm. At least 3 independent experiments were performed, and 20 plants per line were analyzed in each experiment. See also Supplementary Fig. S7A. **B)** Quantification of *P. parasitica* biomass in infected leaves of WT Col-0, *cyp71b3*, CYP71B3 CM lines (CM-1 and CM-2), and OE lines (OE-1 and OE-2) at hpi was determined by qPCR. The biomass of *P. parasitica* in all lines was normalized with that in WT Col-0 (set to 1). Sample size is 3. Bars represent *PpUBC* levels relative to *AtUBIQUITIN9* levels with SE. Asterisks denote significance analyzed by Student's *t*-test (***$P < 0.001$). **C)** The fluorescence microscopic image of roots of 2-wk-old WT Col-0 and *cyp71b3* plants infected by GFP-tagged *P. parasitica* transformant, at 12 hpi. Scale bar, 200 μm. At least 3 independent experiments were performed, and 10 plants per line were analyzed in each experiment. See also Supplementary Fig. S7B. **D)** Quantification of *P. parasitica* biomass in infected roots of 2-wk-old WT Col-0 and *cyp71b3* plants at 2 hpi was determined by qPCR. The biomass of *P. parasitica* in *cyp71b3* was normalized with that in WT Col-0 (set to 1). Sample size is 3. Bars represent *PpUBC* levels relative to *AtUBIQUITIN9* levels with SE. Asterisks denote significance analyzed by Student's *t*-test (*$P < 0.05$). **E)** ROS burst upon flg22 treatment of leaves of 4-wk-old WT Col-0, *cyp71b3*, CYP71B3 CM lines (CM-1 and CM-2), and OE lines (OE-1 and OE-2). At least 12 leaves from 6 plants of each group were measured using a luminol-based chemiluminescence assay. Data presented show means ± SD. Three independent experiments were repeated with similar results. **F)** Quantification of bacterial growth in indicated plants following infiltration of virulent bacterial pathogens *P. syringae* pv. *tomato (Pst)* DC3000 (4×10^5 CFU/mL). At least 3 independent experiments were performed, and 20 plants per line were analyzed. Error bars indicate ± SD. Asterisks denote significance analyzed by Student's *t*-test (*$P < 0.05$, **$P < 0.01$). RLU, relative light units.

Boller 2000) was measured in leaves of Col-0, *cyp71b3* mutants, CYP71B3-CM, and CYP71B3-OE lines. In contrast to Col-0, the oxidative burst was attenuated in the *cyp71b3* mutant plants, whereas both CYP71B3-CM lines showed a comparable level of oxidative burst to Col-0, and a stronger oxidative burst occurred in both CYP71B3-OE lines (Fig. 3E). Taken together, these results indicate that *CYP71B3* positively affects PAMP-triggered ROS production in plant.

The ER membrane-associated CYP71B3 interacts with and is destabilized by RTP1

Given that the majority of CYP71 family proteins are predicted to be localized in the ER membrane system (Neve and Ingelman-Sundberg 2010), we investigated the subcellular localization of CYP71B3 in *N. benthamiana* leaves cotransformed with 35S::*GFP-CYP71B3* and 35S::*RFP-ER*. Confocal laser scanning micrographs revealed the co-localization of GFP-CYP71B3 and RFP-ER (Fig. 4, A and B), and the expression and integrity of GFP-CYP71B3 was confirmed by western blot (Supplementary Fig. S8B), indicating that CYP71B3 was localized to the ER. This prompted us to investigate whether CYP71B3 might interact with RTP1. Using a firefly luciferase complementation imaging (LCI) assay, we analyzed the protein interaction between the RTP1 and CYP71B3, in which the ER membrane-associated proteins Bax inhibitor-1 (BI-1) (Xu and Reed 1998; Chae et al. 2003; Qiang et al. 2021) and CYP71B20 (Neve and Ingelman-Sundberg 2010) were used as a negative control. Notably, coexpression of RTP1-NLuc with either CLuc or CLuc-CYP71B20, as well as the BI-1-NLuc with CLuc, did not show luciferase CM signals, whereas coexpression of RTP1-NLuc and CLuc-CYP71B3 exhibited strong luciferase CM signals (Fig. 4C; Supplementary Fig. S9A). These results imply that the CYP71B3 protein might interact with RTP1.

To confirm this interaction, we carried out coimmunoprecipitation (Co-IP) assays. The 35S::*CYP71B3-mCherry* construct was co-transformed with either 35S::*RTP1-FLAG* or 35S::*FLAG-GFP* into *N. benthamiana* leaves by agroinfiltration. The immunoblotting results showed that CYP71B3-mCherry was coimmunoprecipitated in RTP1-FLAG–expressed samples, but not in FLAG-GFP samples (Fig. 4D; Supplementary Fig. S10), though the construct was expressed in all leaves. These results indicated that RTP1 interacts with CYP71B3.

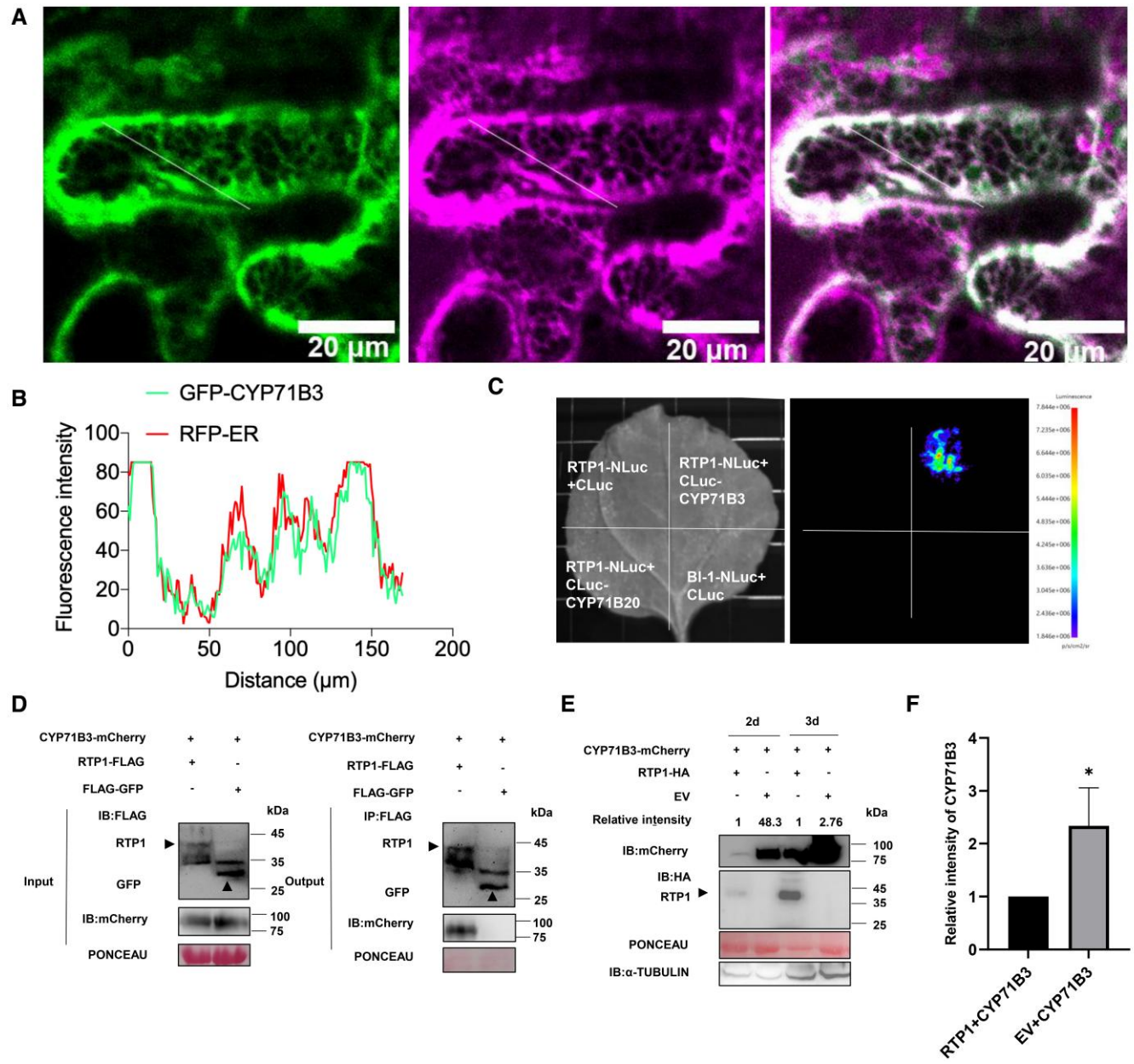

Figure 4. RTP1 interacts with and destabilizes the ER membrane-associated CYP71B3. **A** and **B)** CYP71B3 was colocalized with ER marker protein. GFP-CYP71B3 and RFP-ER were coexpressed in *N. benthamiana* leaves. At 48 h, the distribution of fluorescence in *N. benthamiana* epidermal cells transiently expressing GFP-CYP71B3 and RFP-ER was observed by confocal microscopy. Scale bars, 20 μm. **C)** Protein interaction between RTP1 and CYP71B3 in living cells was detected by firefly LCI assay at 72 h postinfiltration. Coexpression of RTP1-NLuc and CLuc-CYP71B3 resulted in specific fluorescence as detected by a low-light cooled charge–coupled device camera. Three independent biological experiments were performed and showed similar results. See also Supplementary Fig. S9A. **D)** Co-IP assays showing RTP1 interaction with CYP71B3. Total native protein extracts (input) from agroinfiltrated leaves expressing the indicated proteins were precipitated with anti-FLAG M2 affinity gel (IP:FLAG), separated on SDS–PAGE gels, and blotted with specific antibodies. In immunoprecipitation fractions, CYP71B3-mCherry was detected in a complex with RTP1-3*FLAG, but not with FLAG-GFP. Protein size markers were indicated in kDa, and protein loading was indicated by Ponceau S staining. Three independent experiments were performed and showed similar results. See also Supplementary Fig. S10. **E)** Protein stability of CYP71B3, coexpressed with RTP1 or EV, was analyzed by immunoblotting (IB). Total proteins were extracted from infiltrated leaves at 2 and 3 d postinfiltration. The accumulation of CYP71B3-mCherry and RTP1-HA was detected by IB using anti-mCherry and anti-HA antibodies, respectively. Anti-TUBULIN was used to show equal protein concentration, and Ponceau S staining of the membrane was used to show equal loading. Three independent experiments were performed and showed similar results. See also Supplementary Fig. S11. **F)** The relative intensity of CYP71B3 (protein accumulation at 3-d postinfiltration, when coexpressed CYP71B3-mCherry and RTP1-HA, was set to 1) in 3 independent protein stability assays were determined by Image J. See also Supplementary Fig. S11. Error bars indicate ± SD of 3 biological replicates. Asterisks denote significance analyzed by Student's *t*-test (*$P < 0.05$).

To further evaluate whether RTP1 might affect the stability of CYP71B3, the 35S::*CYP71B3-mCherry* construct was cotransformed with 35S::*RTP1-HA* or the empty vector (EV) into *N. benthamiana* leaves by agroinfiltration. At 2 and 3 dpi, the leaf proteins were extracted, and an equal amount of protein per sample was used to evaluate the impact of RTP1 on CYP71B3 protein stability. Immunoblotting analysis revealed that CYP71B3 accumulation was significantly reduced when coexpressed with RTP1 compared with that of the EV. Particularly, a decrease of 57% accumulation of CYP71B3 protein was observed at 3 dpi (Fig. 4, E

and F; Supplementary Fig. S11). These results indicate that the ER membrane-associated protein CYP71B3 could be destabilized by RTP1.

I-38 is crucial for CYP71B3 protein interaction with RTP1

Next, we investigated which site of CYP71B3 might be crucial for its interaction with RTP1. Through phylogenetic analyses on the coding sequences of *CYP71* family genes of *Arabidopsis* (Supplementary Fig. S12A) via MEME (http://meme-suite.org/tools/meme; Supplementary Methods S2), 3 conserved functional motifs were identified, among which the motif LPPXXXPXIGNL HQLXXXPHR was the most significantly conserved (E-value = 7.33e-59), as demonstrated by its location (at position AA29 to AA45) in CYP71B3 protein (Fig. 5A). We hypothesized this conserved motif of CYP71B3 might be essential for its interaction with RTP1. To test this, we first confirmed the protein expression of CYP71B3$^{\Delta AA29\ to\ AA45}$ -mCherry by western blot (Supplementary Fig. S8A) and then agroinfiltrated constructs of RTP1-NLuc and CLuc-CYP71B3$^{\Delta AA29\ to\ AA45}$, RTP1-NLuc and CLuc-CYP71B3, RTP1-NLuc and CLuc as well as NLuc and CLuc-CYP71B3 into leaves of *N. benthamiana*, followed by LCI assay. Expectedly, we found luciferase CM signals in leaf areas coexpressing RTP1-NLuc and CLuc-CYP71B3. However, this signal was not observed when RTP1-NLuc was coexpressed with CLuc-CYP71B3$^{\Delta AA29\ to\ AA45}$ (Fig. 5B; Supplementary Fig. S9B). These results indicate that the LPPXXXPXIGNLHQL motif of CYP71B3 protein is essential for its interaction with RTP1.

To further identify the key functional site of CYP71B3 for interaction with RTP1, we subsequently analyzed the interaction between RTP1 and several other CYP71 family proteins, including CYP71B22, CYP71A12, CYP71A13, and CYP71B20, with CYP71B3 as a control, using LCI assay. We observed that coexpression of RTP1-NLuc and CLuc-CYP71B22 or CLuc-CYP71B3 also resulted in luciferase CM signals, but not the coexpression of RTP1-NLuc with CLuc-CYP71A12, CLuc-CYP71A13, or CLuc-CYP71B20 (Supplementary Fig. S12, B to F). Sequence alignment of the LPPXXXPXIGNLHQL motif in CYP71B3, CYP71B22, CYP71A12, CYP71A13, and CYP71B20 proteins showed that the amino acid residue I38 was unique to RTP1-interacting CYP71B3 and CYP71B22 (Fig. 5C). Prediction of protein structures of CYP71B3 (Qmean=0.68) and CYP71B22 (Qmean=0.71), respectively, using SPPIDER database (http://sppider.cchmc.org/) further revealed that I38 residue is exposed on the protein surface (Fig. 5D; Supplementary Fig. S13).

To confirm whether the I38 residue of CYP71B3 is vital for protein interaction between CYP71B3 and RTP1, we generated a point mutation by replacing I38 with A38 and confirmed that the CYP71B3$^{(I38A)}$ protein could normally express (Fig. 5F). Thereafter, we performed a LCI assay in *N. benthamiana* leaves to analyze the interaction between RTP1-NLuc and CLuc-CYP71B3$^{(I38A)}$, RTP1-NLuc and CLuc-CYP71B3, NLuc and CLuc-CYP71B3$^{(I38A)}$ as well as RTP1-NLuc and CLuc. Coexpression of RTP1-NLuc and CLuc-CYP71B3 showed luciferase CM signals, whereas the signal disappeared when RTP1-NLuc and CLuc-CYP71B3$^{(I38A)}$ were coexpressed. Similarly, coexpression of NLuc and CLuc-CYP71B3$^{(I38A)}$, as well as RTP1-NLuc and CLuc did not show luciferase CM signals (Fig. 5E; Supplementary Fig. S9C). To confirm the role of I38 residue of CYP71B3 in the interaction with RTP1, the 35S::*CYP71B3*$^{(I38A)}$*-mCherry* was cotransformed with either 35S::*RTP1-FLAG* or 35S::*FLAG-GFP* into *N. benthamiana* leaves by agroinfiltration, for Co-IP assays. The immunoblotting results showed that CYP71B3$^{(I38A)}$-mCherry could not be coimmunoprecipitated in either RTP1-FLAG–expressed or FLAG-GFP samples (Fig. 5F), though the fusion proteins were expressed in all leaves. Together, these results indicate that the I38 residue of CYP71B3 is essential for its interaction with RTP1.

Intriguingly, based on the prediction of the protein tertiary structure of RTP1 via TASSER (https://zhanggroup.org/) (C-score=-1.39) and CYP71B3 via SWISS-MODEL (https://swissmodel.expasy.org/) (Qmean=0.68) (Supplementary Fig. S14, A and B), we performed virtual protein docking between RTP1 and CYP71B3 using ZDOCK (http://zdock.umassmed.edu/) and showed that the I38 residue of CYP71B3 might interact with RTP1 (Supplementary Fig. S14C). To further examine whether the I38 residue affects the destabilization of CYP71B3 by RTP1, we cotransformed 35S::*CYP71B3*$^{(I38A)}$*-mCherry* with 35S::*RTP1-HA* or the 35S::*FLAG-GFP* into *N. benthamiana* leaves by agroinfiltration. At 3 dpi, the immunoblotting analysis showed that, in contrast to the dramatic attenuation of CYP71B3 accumulation in the presence of RTP1 (Fig. 4E; Supplementary Fig. S15), the protein accumulation of CYP71B3$^{(I38A)}$ was not significantly altered when coexpressed with RTP1 (Fig. 5, G and H; Supplementary Fig. S15). Collectively, these results support the notion that the I38 residue is vital for the interaction of CYP71B3 with RTP1.

I-38 residue is crucial for the immune function and P450 enzyme activity of CYP71B3

To further explore the role of I38 residue, the key interacting site of CYP71B3 with RTP1, in the immune function of CYP71B3, we performed genetic CM of *cyp71b3* with CYP71B3$^{(I38A)}$. The CYP71B3$^{(I38A)}$-CM plants showed no obvious changes in growth or morphology when compared with Col-0 (Supplementary Fig. S6A). The transcript level of *CYP71B3* in CYP71B3$^{(I38A)}$-CM lines was confirmed by RT-qPCR (Supplementary Fig. S6B). Pathogenicity assays showed that *P. parasitica* colonized *cyp71b3* mutants more rapidly, whereas CYP71B3-CM plants were more resistant than WT Col-0. Notably, the leaves of CYP71B3$^{(I38A)}$-CM plants exhibited larger infection lesions and higher pathogen biomass than those of CYP71B3-CM or WT plants at 3 dpi (Fig. 6, A and B; Supplementary Fig. S7B). These results indicate that the CYP71B3-mediated resistance to *P. parasitica* could be abolished with the I38A point mutation of CYP71B3.

To further examine the impact of CYP71B3$^{(I38A)}$ on flg22-triggered ROS production, we measured the ROS production following flg22 treatment of leaves of Col-0, *cyp71b3* mutant, CYP71B3-CM, and CYP71B3$^{(I38A)}$-CM lines. A typical ROS burst was observed in both WT and CYP71B3-CM plants, while reduced oxidative burst in both *cyp71b3* mutant and CYP71B3$^{(I38A)}$-CM plants was evident (Fig. 6C). These results reveal that the I38 residue, the key interacting site of CYP71B3 with RTP1, is essential for CYP71B3-mediated plant immunity.

Simultaneously, we also examined whether I38 is a functional site for its P450 enzyme activity of CYP71B3. Therefore, histidine-tagged protein constructs were generated, including His-sumo-CYP71B3, His-sumo-CYP71B3$^{(I38A)}$, and His-GFP, and were expressed in vitro and purified. The protein expression was confirmed by SDS–PAGE (Supplementary Fig. S16) before analyzing their relative P450 enzyme activities. The P450 enzyme activity of CYP71B3$^{(I38A)}$ protein was significantly reduced, by ~30% compared with that of the CYP71B3 protein, but still higher than that in the control (Fig. 6D). These results imply that the I38 residue of CYP71B3 protein may be required for its P450 enzyme activity.

Expression of *CYP71B3* is regulated by bZIP60 TF

We previously reported that ER membrane-associated TF bZIP60, one of the key regulators of ER stress signaling, was modulated by

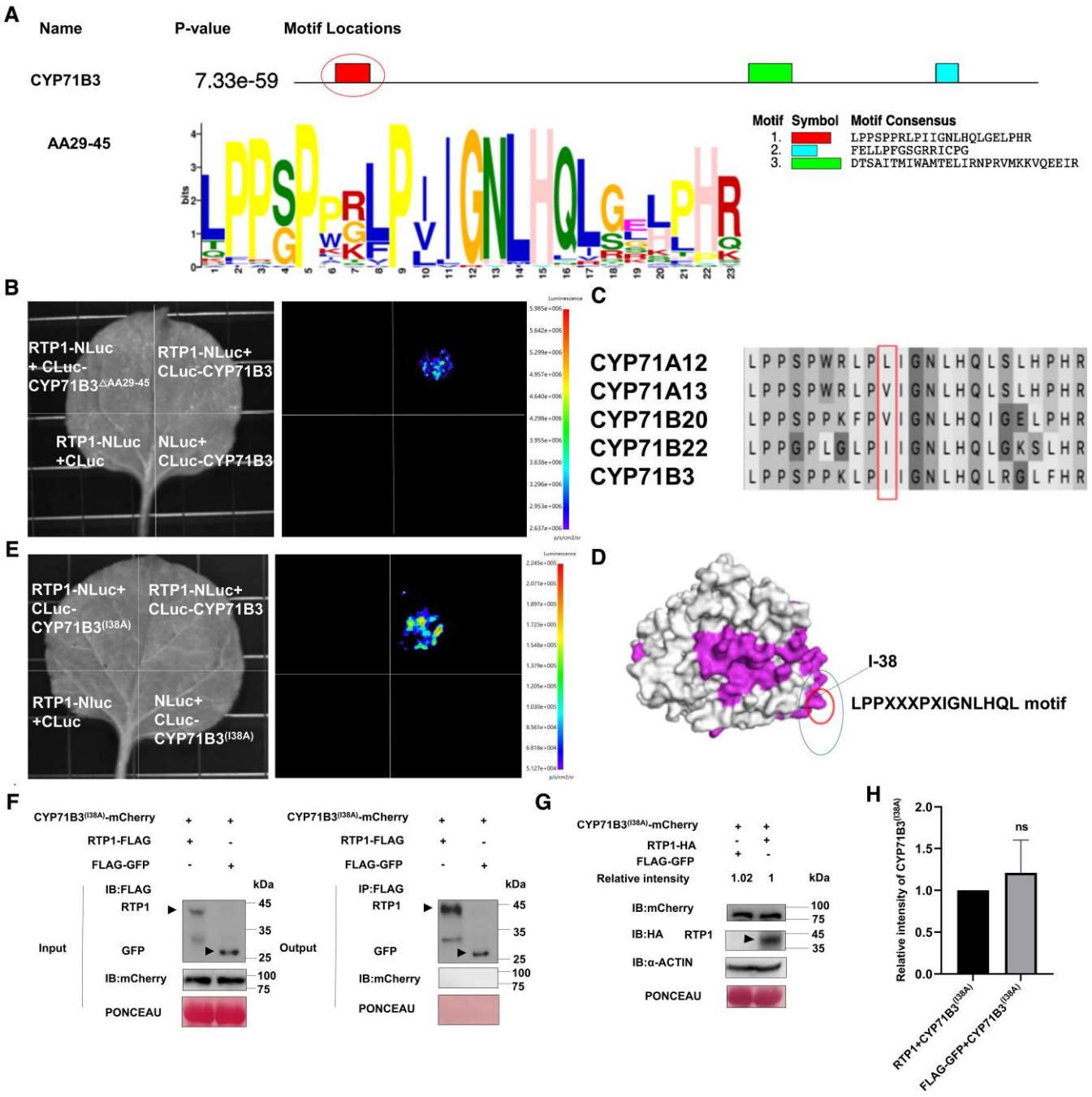

Figure 5. The I-38 residue of CYP71B3 protein is vital for interaction with RTP1. **A)** The prediction of conserved motifs in N terminus of CYP71B3 protein using MEME (http://meme-suite.org/tools/meme). The circle represents the position of the motif. **B)** The interaction between RTP1 and CYP71B3$^{\Delta AA29\text{-}AA45}$ in *N. benthamiana* epidermal cells transiently expressing RTP1-NLuc with CLuc-CYP71B3$^{\Delta AA29\text{-}AA45}$ or CLuc-CYP71B3 or CLuc, and NLuc with CLuc-CYP71B3 was detected by firefly LCI assay at 72 h postinfiltration. Three independent biological experiments were performed and showed similar results. See also Supplementary Fig. S9B. **C)** Sequence alignment of conserved motifs of several CYP71 family proteins either interacting with or not interacting with RTP1. The red box represents the position of I38 amino acid residue in several CYP71 family proteins. **D)** The prediction of I-38 residue and LPPXXXPXIGNLHQL motif via SPPIDER (http://sppider.cchmc.org/). The blue circle represents the position of the motif. The red circle represents the position of I38 amino acid residue. **E)** The interaction between RTP1 and CYP71B3 $^{(I38A)}$ in *N. benthamiana* epidermal cells transiently expressing RTP1-NLuc with CLuc-CYP71B3$^{(I38A)}$ or CLuc-CYP71B3 or CLuc, and NLuc with CLuc-CYP71B3$^{(I38A)}$ was detected by firefly LCI assay at 72 h postinfiltration. Three independent biological experiments were performed and showed similar results. See also Supplementary Fig. S9C. **F)** Co-IP assays showing no protein interaction between RTP1 and CYP71B3$^{(I38A)}$. Total native protein extracts (input) from agroinfiltrated leaves expressing the indicated proteins were precipitated with anti-FLAG M2 affinity gel (IP:FLAG), separated on SDS–PAGE gels, and blotted with specific antibodies. In immunoprecipitation fractions, CYP71B3$^{(I38A)}$-mCherry was neither detected in a complex with RTP1-3*FLAG, nor FLAG-GFP. Protein size markers were indicated in kDa, and protein loading was indicated by Ponceau S staining. Three independent biological experiments were performed and showed similar results. **G)** Protein stability of CYP71B3$^{(I38A)}$, coexpressed with RTP1 or FLAG-GFP, was analyzed by immunoblotting (IB). The accumulation of CYP71B3$^{(I38A)}$-mCherry and RTP1-HA was detected by IB using anti-mCherry and anti-HA antibodies, respectively. Three independent biological experiments were performed and showed similar results. See also Supplementary Fig. S15. **H)** The relative intensity of CYP71B3$^{(I38A)}$ in 3 independent biological protein stability assays was quantified. Relative CYP71B3$^{(I38A)}$ protein band intensities (protein accumulation at 3-d post infiltration, when coexpressed CYP71B3$^{(I38A)}$-mCherry and RTP1-HA, was set to 1) were determined by Image J. See also Supplementary Fig. S11. Error bars indicate ± SD of 3 biological replicates. Asterisks denote significance analyzed by Student's *t*-test (*$P < 0.05$).

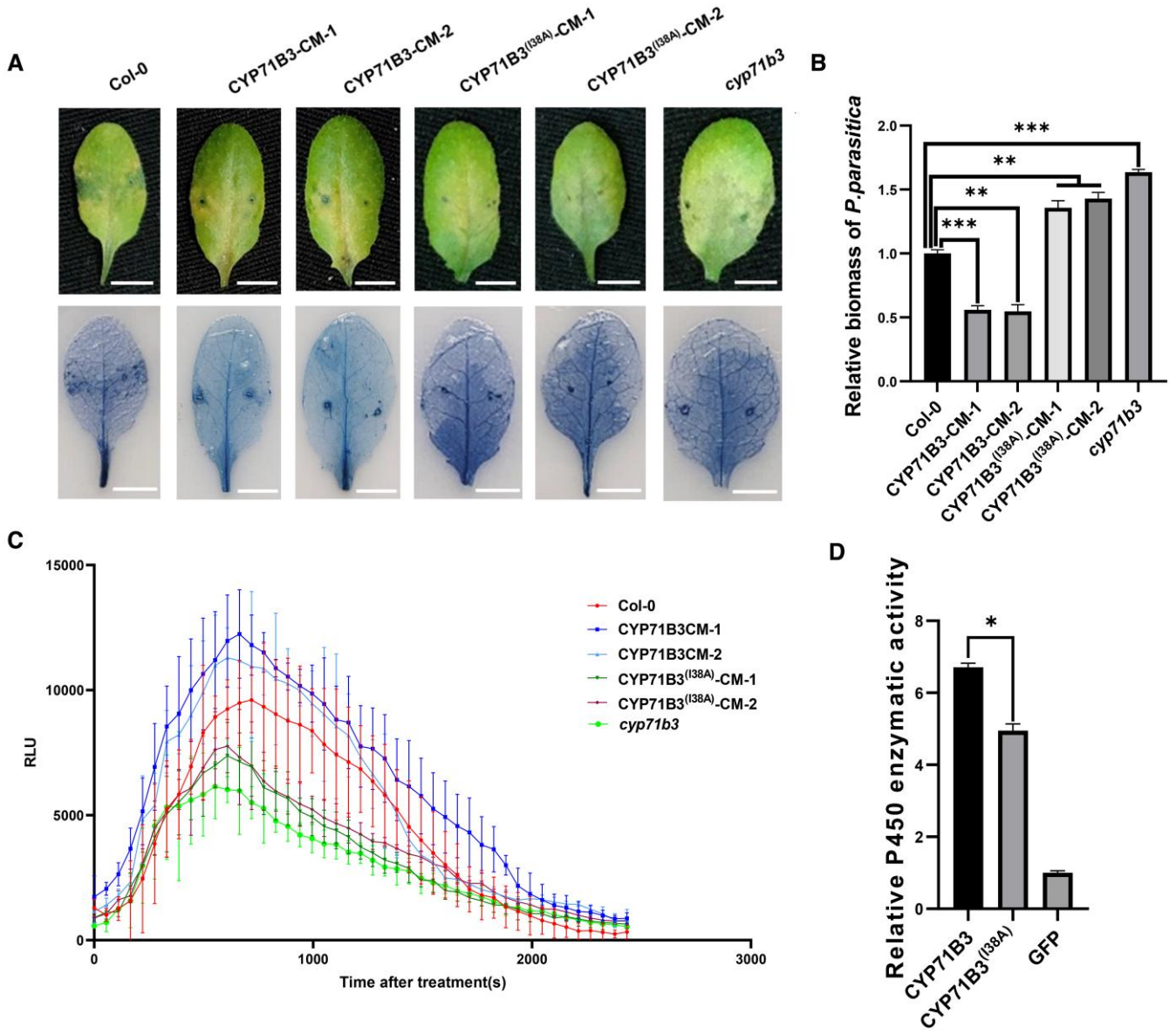

Figure 6. The I-38 residue of CYP71B3 protein is vital for its immune function. The point mutation of I38A abolished CYP71B3-mediated resistance to *P. parasitica*. **A)** Detached leaves of 4-wk-old indicated plants were inoculated with *P. parasitica* zoospores. The water-soaked lesions with trypan blue staining were recorded at 3 d past inoculation (dpi). Scale bar, 0.5 cm. At least 3 independent biological experiments were performed, and 20 plants per line were analyzed in each experiment. See also Supplementary Fig. S7C. **B)** *P. parasitica* biomass was determined by qPCR at hpi. The *P. parasitica* biomass in all lines was normalized with that in WT Col-0 (set to 1). Sample size is 3. Bars represent *PpUBC* levels relative to *AtUBIQUITIN9* levels with SD. Asterisks denote significance analyzed by Student's *t*-test (***$P < 0.001$). **C)** ROS burst upon flg22 treatment of leaves of 4-wk-old WT Col-0, *cyp71b3*, CYP71B3-CM, and CYP71B3$^{(I38A)}$-CM lines. Sample size is 10. Data presented show means ± SD. **D)** The P450 enzyme activities of CYP71B3 and CYP71B3 $^{(I38A)}$. The absorbance at 370 nm was measured to indicate P450 enzyme activity. Data shown represent the relative P450 enzyme activities and displayed the ratio of relative fluorescence units (RFUs) of CYP71B3 or CYP71B3$^{(I38A)}$ to GFP. Data presented show means of 3 independent experiments ± SE. Asterisk indicates significance at $P < 0.05$ (*) analyzed by Student's *t*-test.

RTP1 and required for *rtp1* resistance to *P. parasitica* (Qiang et al. 2021). Through analyzing the promoter sequence of *CYP71B3* using plantCARE (http://bioinformatics.psb.ugent.be/webtools/plantcare/html/), we found 2 W-box core cis-elements (TTGACC) and a C-box core cis-element (GACGTC) (Fig. 7A), which were thought to be required for binding to bZIP60 TF (Jakoby et al. 2002; Sun et al. 2013). Through analyses on the expression of *CYP71B3* in Col-0 and *bzip60* mutant plants upon early colonization of *P. parasitica*, we found its expression was strongly reduced in *bzip60* mutants when compared with WT at 12 hpi, indicating the expression of *CYP71B3* is regulated by bZIP60 TF (Fig. 7B).

To examine the effect of bZIP60 TF on activating the transcription of *CYP71B3*, we performed a dual-luciferase reporter assay. A mixture of *A. tumefaciens* GV3101 cells containing either bZIP60ΔC or EV and the *CYP71B3* promoter was infiltrated into leaves of *N. benthamiana* and luciferase activity was analyzed. The results showed a ∼4-fold increase in luciferase activity when bZIP60ΔC and promoter of *CYP71B3* were coinfiltrated (Fig. 7, C and D), indicating that the activated form of bZIP60 TF could transactivate the promoter of *CYP71B3*. We further performed yeast 1-hybrid (Y1H) assay to investigate whether the activated form of bZIP60 TF could bind to the promoter of *CYP71B3*. The results showed that bZIP60ΔC could physically bind to the *CYP71B3* promoter

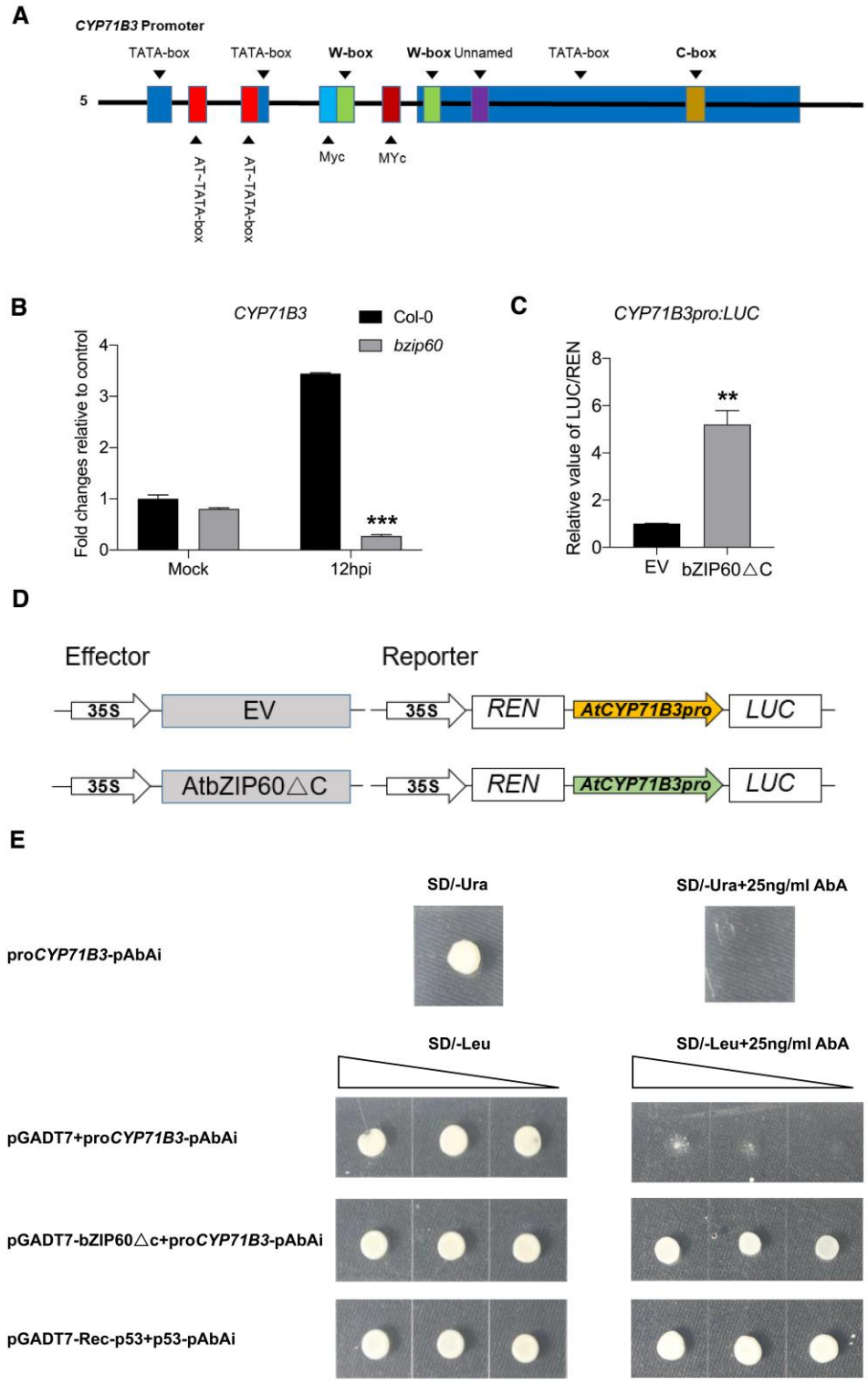

Figure 7. Expression of *CYP71B3* is regulated by TF bZIP60. **A)** Prediction of regulatory elements in the promoter of *CYP71B3* via plantCARE (http://bioinformatics.psb.ugent.be/webtools/plantcare/html/). The W-box and C-box elements were indicated. The cube's size means the length of indicated regulatory elements, and each color represents the type of the regulatory elements. **B)** Expressions of *CYP71B3* in WT Col-0 and *bzip60* mutant plants were determined by RT-qPCR. Two-week-old roots were dip-inoculated by *P. parasitica* zoospores or mock solution and harvested at 12 hpi. Data presented show means of 3 independent experiments ± SD. Asterisks indicate significance at $^{***}P < 0.001$ analyzed by Student's *t*-test. **C** and **D)** *CYP71B3* promoter-LUC activity was determined by dual-luciferase reporter assay. A mixture of *A. tumefaciens* containing either bZIP60ΔC or 62SK EV and *CYP71B3* promoter were infiltrated into leaves of *N. benthamiana*. At 48 h, firefly luciferase (LUC) and renilla (REN) luciferase were assayed. The ratio of LUC/REN to the EV with promoter was used as a calibrator (set as 1). The experiments were performed 3 times with similar results. The bars represent means ± SD and the asterisks indicate significant differences ($^{*}P < 0.05$; $^{**}P < 0.01$) analyzed by Student's *t*-test. **E)** Y1H assays on the interaction of bZIP60ΔC with the promoter of *CYP71B3*. Oblique triangles above the images indicated as 1, 0.5, and 0.1 yeast-cell concentration gradient.

(Fig. 7E). These results confirmed that the activated form of bZIP60 TF could bind and activate the promoter of *CYP71B3* gene.

Discussion

An effective strategy that could be employed to enhance crop durable disease resistance is to modify susceptibility genes, which are required for the virulence or pathogenicity of pathogens (Pavan et al. 2010). Taken the wheat receptor-like cytoplasmic kinase gene *Puccinia striiformis-induced protein kinase 1* (*TaPsIPK1*) as an example, its inactivation via CRISPR-Cas9 could confer wheat broad-spectrum resistance to rust fungi without fitness penalty (Wang et al. 2022). Nevertheless, in order to be more precisely utilized in molecular resistance breeding, the mechanism of how susceptibility genes negatively regulate plant immunity remained to be deciphered.

Our findings that *RTP1* loss-of-function resulted in the upregulation of several *CYP71* family genes including *CYP71B3* (Fig. 1, B and C), and that OE of *CYP71B3* relieved *RTP1*-mediated susceptibility to *P. parasitica* (Figs. 2, A to C and 3, A to D; Supplementary Fig. S5, A and B) and the absence of *CYP71B3* compromised *rtp1* resistance to *P. parasitica* (Figs. 2, D and E and 3, A to D) point to the notion that CYP71B3 plays a pivotal role in plant immune signaling mediated by RTP1. Further pathogenicity assays confirmed its positive regulatory role in resistance against *P. parasitica* as well as biotrophic bacterial pathogen *P. syringae* (Fig. 3F). Intriguingly, *CYP71B3* expression was shown to be induced upon infection by multiple other hemibiotrophic or biotrophic pathogens, but not necrotrophic pathogens (Scholz et al. 2018; Liu et al. 2015; Supplementary Fig. S4C), which provided further evidence of its association with *RTP1*. Notably, our findings that *CYP71B3* expression could be induced upon flg22 treatment (Supplementary Fig. S4, A and B; Rallapalli et al. 2014) and positively modulates flg22-induced ROS burst (Fig. 3E) as well as the expression of flg22-responsive immune genes *WRKY33* and *FRK1* upon infection (Supplementary Fig. S17) indicate that *CYP71B3* plays a positive regulatory role in PAMP-triggered immunity. Interestingly, *CYP71B3* was also shown to be significantly induced by abiotic stress stimuli such as salt and heat (*Arabidopsis* RNA-seq Database) (Zhang et al. 2020; Supplementary Fig. S4D). Taken together, these results shed light on the potential contribution of *CYP71B3* in plant response to broad-spectrum pathogens and abiotic stresses.

Through analyzing the motifs of CYP71 family proteins, we identified a highly conserved motif (LPPXXXPXIGNLHQL) at the N terminus of CYP71 family proteins (Fig. 5A). Further studies revealed that CYP71B3 could interact with and be destabilized by RTP1 (Fig. 4, C to E), for which the I38 residue within this motif (AA29 to 45) was essential (Fig. 5, B to G). Notably, our investigations demonstrated that the I38 residue was also essential for both immune function and P450 enzyme activity of the CYP71B3 protein (Fig. 6, A to D). As the protein docking analysis supports the possibility that RTP1 might interact with CYP71B3 via I38 (Supplementary Fig. S14), we speculate that the enzyme activity pocket of CYP71B3 (Supplementary Fig. S18) might be blocked during the interaction with RTP1, the outcome of which might manipulate the immune function of CYP71B3. It is also worth noting that the identification of this key site might facilitate enzyme engineering and to improve the enzymatic activity of CYP71B3 against pathogens. Meanwhile, some CYP71 proteins are anchored to the ER membrane via an N-terminal transmembrane helix (predicted for CYP71B3). I38 is near this helix and is modeled to be surface-exposed in a loop with other hydrophobic residues. An alternative hypothesis for the loss of RTP1 association and immune phenotype could be the loss of ER localization. In addition, sccording to ZDOCK result, the Arg7 of RTP1 is closest in spatial position to Ile38 of CYP71B3 (Figure S14), we therefore speculate they may interact with. However, their interaction needs to be confirmed.

To further explore the evolutionary significance of the LPPXXXPXIGNLHQL motif, we performed phylogenetic analysis of *Arabidopsis* CYP450 proteins and found its unique in CYP71 family proteins, being the highly conserved genes among cytochrome P450 (CYPs) (Supplementary Fig. S19, A and B). Moreover, we found that AtCYP71B3 was in the same phylogenetic branch with those of *Solanaceae* plants, but was distinct from OsCYP71B3, ZmCYP71B3, and TaCYP71B3 (Supplementary Fig. S19C). Intriguingly, LPPXXXPXIGNLHQL motif sequence alignment indicated the existence of I38 in SlCYP71B3 and StCYP71B3, but not in OsCYP71B3, ZmCYP71B3, and TaCYP71B3 (Supplementary Fig. S19D). It might be interesting to examine the immune function of CYP71B3 in respective crop plants, which could facilitate our understanding of the functional evolution of this conserved motif.

There are substantial evidences that many *CYP71* family genes contribute to *Arabidopsis* immunity by catalyzing camalexin biosynthesis (Glawischnig 2006). Nevertheless, we found almost unaltered amount of camalexin in *cyp71b3* relative to WT Col-0 upon infection by *P. parasitica* (Supplementary Fig. S20 and Methods S1). . The metabolic pathway in which CYP71B3 is involved still requires further investigation. Nevertheless, given that the P450 enzymes including CYP71B15 (PAD3), CYP71A12, CYP71A13, CYP79B2, and ATR1 could form a complex in the ER and participate in the process of camalexin synthesis in *Arabidopsis* (Mucha et al. 2019), we assume one possibility that CYP71B3 might function redundantly with camalexin biosynthetic genes.

In previous studies, we demonstrated that the susceptibility factor RTP1 could synergistically modulate bZIP60 TF, an important ER stress response regulator, to negatively regulate plant resistance to *P. parasitica* (Qiang et al. 2021). Intriguingly, we found that the induction of *CYP71B3* was strongly reduced in *bzip60* mutants during the early colonization of *P. parasitica* (Fig. 7B), and further assays indicated the binding of bZIP60 TF to the promoter of *CYP71B3* (Fig. 7, C and E). These results support the notion that bZIP60 TF plays a regulatory role in the expression of *CYP71B3*. As RTP1 was demonstrated to stabilize the ER membrane-associated bZIP60 through manipulating the bifunctional protein kinase/ribonuclease IRE1-mediated bZIP60 splicing activity (Qiang et al. 2021), one explanation is that RTP1 retains bZIP60 in the ER, which consequently manipulates the expression of *CYP71B3* regulated by the activated form of bZIP60 TF. Intriguingly, our findings that the induction of UPR marker gene *Binding Protein 3* (*BiP3*) and ER stress sensor gene *bZIP28* in *P. parasitica*-infected WT Col-0 (12 hpi) was significantly attenuated in *cyp71b3* mutant (Supplementary Fig. S21) indicated a role of *CYP71B3* in UPR signaling upon early infection by *P. parasitica*.

Collectively, we identified *CYP71B3* as an important downstream immune factor of the susceptibility factor *RTP1*, which is regulated by the bZIP60 TF. It positively affects plant resistance to multiple pathogens. Intriguingly, the protein encoded by *CYP71B3* interacts with and is destabilized by RTP1 via the I38 residue, which is also essential for its immune function and P450 enzyme activity (Fig. 8). Taken together, our studies not only demonstrate that the susceptibility factor RTP1 negatively regulates plant broad-spectrum disease resistance by interacting with and destabilizing CYP71B3, a positive immune regulator, but also expand our understanding as to the dual function of ER membrane-associated bZIP60 in ER stress response and plant immunity.

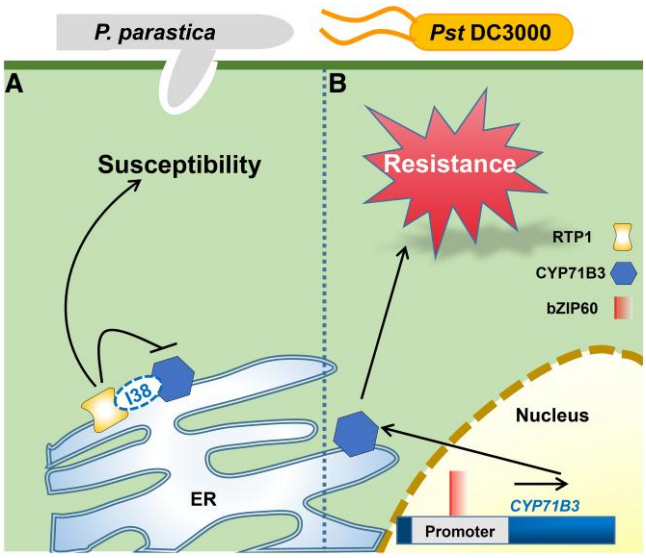

Figure 8. A schematic model showing suppression of CYP71B3-mediated plant immunity by the susceptibility factor RTP1 in *Arabidopsis*. Our studies identified CYP71B3 as an important downstream immune factor of the susceptibility factor RTP1, whose transcription is activated by the bZIP60 TF. CYP71B3 positively regulates plant resistance to multiple pathogens, including the oomycete pathogen *P. parasitica* and bacterial pathogen *P. syringae* pv. *tomato* DC3000. RTP1 interacts directly and destabilizes CYP71B3 via the I38 residue, which is essential for its immune function and P450 enzyme activity. We propose that RTP1 enhances plant susceptibility by directly interacting with and destabilizing CYP71B3 **A)**, while in the *rtp1* plants, CYP71B3-mediated resistance to broad-spectrum pathogens is activated **B)**.

Materials and methods

Plant materials, growth conditions, and plant inoculation

The *CYP71B3* T-DNA insertion line (SALK_008912C) was obtained from AraShare (a nonprofit *Arabidopsis* share center, http://www.AraShare.cn). The T-DNA insertion homozygous mutants were confirmed by PCR using primers *cyp71b3*-LP, *cyp71b3*-RP, and LBb1.3 (Supplementary Table S2). For root inoculation, all *Arabidopsis* seeds were sterilized and grown in squared dishes on half-strength MS. For leaf inoculation on leaves of *A. thaliana*, the plant growing conditions were as previously described (Pan et al. 2016). The culture and zoospore production of *P. parasitica* were conducted as previously described (Wang et al. 2011). The concentration of zoospores was adjusted to 10^5 zoospores/mL unless otherwise specified. The detached leaf inoculation was conducted as previously described (Qiang et al. 2021). For the quantitation of infection, genomic DNA was extracted by the CTAB method. The method to quantify the pathogen's biomass was conducted as previously described (Pan et al. 2016).

The bacterial pathogen *P. syringae* pv. *tomato (Pst)* DC3000 was cultured as previously described (Pan et al. 2016). The final concentration of 4×10^5 CFU mL^{-1} was used for bacterial growth assays.

RNA sequencing and data analysis

Total RNA was isolated from leaves of 8-wk-old *Arabidopsis* roots of WT Col-0 and *rtp1* with either mock treatment or *P. parasitica* inoculation at 3 and 6 hpi, respectively, by RNA extraction kit (DP432, Tiangen, Beijing, China) and sequenced with an Illumina HiSeq4000 PE150 at Novogene Bioinformatics Technology Corporation (Beijing, China) to generate 150 bp paired-end reads (Wang et al. 2009). Three replicates were prepared for each sample. For gene expression analysis, all reads were returned and processed using Trimmomatic software (Bolger et al. 2014) to generate clean data. Clean reads were mapped to the TAIR10 genome by Hisat2 (Kim et al. 2019) and Samtools (Li et al. 2009). featureCounts were used for calculating expression levels (Liao et al. 2014). If the maximum expression value of a gene was more than 1 FPKM among replicated samples of the same treatment, it was defined as an expressed gene; otherwise, it was considered as a nonexpressed one. Among the expressed genes, DESeq2 (Love et al. 2014) was used to identify the DEGs between *rtp1* and Col-0 samples. The genes were defined as upregulated genes ($\log_2$[fold change] ≥ 2, $P \leq 0.05$) and downregulated genes ($\log_2$[fold change] ≤ -2, $P \leq 0.05$), respectively. And, the rest genes were defined as no difference expression genes. To visualize the expression patterns of the candidate genes among the samples, heatmaps and volcano plot were generated using the R package.

Plasmid constructs and plant transformation

For creation of constructs for LCI assay, the coding regions of *RTP1*, *CYP71B3*, *CYP71B22*, *CYP71A12*, *CYP71A13*, and *CYP71B20* were cloned from *A. thaliana* Col-0 cDNA and inserted into the KpnI and SalI site of pCAMBIA1300. The sequence of *RTP1* was fused upstream of N-Luc in the pCAMBIA-NLuc vector, and *CYP71B3*, *CYP71B22*, *CYP71A12*, *CYP71A13*, and *CYP71B20* were fused downstream of C-Luc in the pCAMBIA-CLuc vector. For transient expression assays and *A. thaliana* genetic transformation, a full-length coding sequence of *CYP71B3* was cloned from *A. thaliana* cDNA. The amplified fragment was ligated into pKannibal with *XhoI* and *XbaI* sites and then inserted into the binary vector pART27 (Gleave 1992) at the *NotI* site. To create mCherry-fusion, the mCherry fragment was cloned into pKannibal with *XhoI* and *XbaI* sites and *Not1* sites were used to release the fragment with the promoter and terminator and then inserted into the binary vector pART27. The coding sequences of *CYP71B3* and $CYP71B3^{(I38A)}$ were inserted into previously modified pART27 at the *EcoRI* and *Xho1* sites to create CYP71B3-mCherry and $CYP71B3^{(I38A)}$-mCherry. To create GFP-fusion, the GFP fragment was cloned into pKannibal with *XhoI* and *EcoRI* sites and *Not1* sites were used to release the fragment with the promoter and terminator and then inserted into the binary vector pART27. The coding sequence of mature *CYP71B3* was inserted into previously modified pART27 at the *EcoRI* and *Xba1* sites to create GFP-CYP71B3. *CYP71B3* promoter from genomic DNA was inserted into pGreenII 0800-LUC with *BamHI* and *HindIII* sites, and bZIP60ΔC was inserted into pGreenII 0029 62SK vector with *BamHI* and *PstI* sites. In order to make the *proCYP71B3::CYP71B3* and *proCYP71B3::*$CYP71B3^{(I38A)}$ fusion, a 371-bp promoter fragment of *CYP71B3* was amplified from Col-0 genomic DNA and inserted into vector pART27 with *SpeI* and *XbaI* sites and $CYP71B3^{(I38A)}$ or *CYP71B3* inserted into *SpeI* site of pART27::*proCYP71B3*. The primers used above were listed in Supplementary Table S2.

The constructs were transformed into *Arabidopsis* by *A. tumefaciens*-mediated transformation using the floral dipping method (Zhang et al. 2006; Narusaka et al. 2010) . The generated transformants were confirmed by both antibiotic resistance and genotyping. Two independent T3 homozygous lines were used for further experiments.

Gene expression analysis

Four-week-old leaves or 2-wk-old roots of *Arabidopsis* with inoculation or mock treatment were collected to extract total RNA using TRIzol reagent (Invitrogen) according to the manufacturer's instructions. The gene expression was analyzed by RT-qPCR as described (Qiang et al. 2021). Primers used were listed in Supplementary Table S2.

Agroinfiltration and confocal laser scanning microscopy

A. tumefaciens GV3101 carrying constructs were grown at 28 °C for 36 h in LB medium with appropriate antibiotics. *Agrobacteria* were collected by centrifugation and resuspended in infiltration buffer (10 mM MES, 10 mM $MgCl_2$, and 200 mM acetosyringone) at OD_{600} = 0.4 and then infiltrated into 4-wk-old *N. benthamiana* leaves. Three days after infiltration, the *N. benthamiana* leaves were examined using an Olympus FV3000 confocal microscope (Japan). GFP was detected after excitation with a 488 nm wavelength laser, and emissions were collected between 500 and 540 nm. The fluorescence of RFP was excited with a 559-nm wavelength laser to detect specific emissions between 600 and 680 nm.

Firefly LCI assay

The constructed vectors were transformed into *Agrobacterium* strain GV3101 and then infiltrated *N. benthamiana* leaves (OD_{600} = 0.4). After 3 d, 1 mM beetle luciferin (Promega) was sprayed on leaves and kept dark for 6 min at room temperature to quench the autofluorescence. A low-light cooled charge–coupled device camera (Lumazone Pylon 2048B, Princeton, NJ, USA) was used to capture the LUC image (Chen et al. 2008).

Co-IP and immunoblot assays

N. benthamiana leaves were harvested at 3 d after agroinfiltration and proteins were extracted with HEPES buffer and Co-IP was performed as described (Win et al. 2011; Qiang et al. 2021). After protein samples were boiled for 5 min, the supernatant was separated on SDS–PAGE gels, and transferred to polyvinylidene fluoride membranes (Roche). Antibodies used for this study included anti-mCherry (AE002, ABclonal; 1:5000), anti-HA (AE008, ABclonal; 1:5000), anti-FLAG (AE063, ABclonal;1:5000), and anti-mouse IgG (AS003, ABclonal; 1:5000). Protein bands were quantified using Image J software (Schneider et al. 2012).

ROS burst assay

The ROS burst was measured as described (Lu et al. 2020). The leaves of 4-wk-old *Arabidopsis* and *N. benthamiana* were selected, and leaf disks were taken from the leaves with a 5 mm puncher. Luminescence of leaves was measured using a TECAN Infinite M200 PRO (TECAN) (cycle number 40, once per minute).

Recombinant protein expression, purification, and P450 enzyme activity assay

The *E. coli* (BL21) carrying recombinant protein□His-sumo-CYP71B3$^{(I38A)}$ □His-sumo-CYP71B3 and His-GFP□ was grown at 37 °C with an OD_{600} of 0.5–0.6 and then incubated with 1 mM isopropyl β-D-1-thiogalactopyranoside at 18 °C for 12 h. Cells were broken and resuspended with ice-cold lysis buffer (50 mM NaH_2PO_4, 300 mM NaCl, 20 mM imidazole [pH 8.0]) containing 1× cocktail (Sigma). Crude proteins were affinity purified by Ni IDA beads (SA003100, Smart-Lifesciences), and the column was washed with buffer containing 50 mM NaH_2PO_4, 300 mM NaCl, and 20 mM imidazole (pH 8.0). Fusion proteins were eluted with elution buffer (50 mM NaH_2PO_4, 300 mM NaCl, 300 mM imidazole [pH 8.0]) and concentrated by centrifugation through an ultrafiltration tube (Merck). The molecular weight of the purified protein was detected by SDS-PAGE and Coomassie Brilliant Blue. The P450 enzyme activities of CYP71B3$^{(I38A)}$ and CYP71B3 were examined following instructions of Biovision P450 enzyme activity assay kit (ID: K895-100) and calculated using a TECAN Infinite M200 PRO (TECAN).

The dual-luciferase reporter assay

All constructs were electroporated into *A. tumefaciens* (pSoup-P19). A mixture of *A. tumefaciens* containing TFs and promoters (OD_{600} = 0.5) was infiltrated into *N. benthamiana* leaves. After 3 d, leaf disks were collected and enzyme activity of firefly and renilla luciferases was measured using YEASEN^{R} dual-luciferase reporter gene assay kit (ID:11402ES60). Three biological replicates were performed for individual experiment.

Y1H assay

Y1H assays were performed following the manual of Matchmaker Gold Y1H System (Clontech, USA). The Coding DNA Sequence (CDS) of AtbZIP60ΔC was cloned and inserted into pGADT7 to construct the prey, and the promoter sequence of *AtCYP71B3* was cloned and inserted into the pAbAi vector to construct the bait, and then were transformed into the Y1H Gold yeast strain. The prey plasmid was introduced into the bait strains. Clones were cultured on selective dropout medium SD/-Leu with or without 25 ng/mL aureobasidin A.

Phylogenetic analyses

The phylogenetic tree was constructed with the MEGA X, aligning the full-length amino acid sequences of CYP71 using the neighbor-joining method for the ClustalW program. The sequences used for the phylogenetic tree included CYP71A18 (AT1G11610), CYP71B2 (AT1G13080), CYP71B29 (AT1G13100), CYP71B7 (AT1G13110), CYP71B9 (AT2G02580), CYP71B6 (AT2G24180), CYP71A12 (AT2G30750), CYP71A13 (AT2G30770), CYP71B16 (AT3G26150), CYP71B17 (AT3G26160), CYP71B19 (AT3G26170), CYP71B20 (AT3G26180), CYP71B21 (AT3G26190), CYP71B22 (AT3G26200), CYP71B23 (AT3G26210), CYP71B3 (AT3G 26220), CYP71B24 (AT3G26230), CYP71B25 (AT3G26270), CYP71B33 (AT3G26295), CYP71B34 (AT3G26300), CYP71B35 (AT3G26310), CYP71B36 (AT3G26320), CYP71B37 (AT3G26330), CYP71B15 (AT3G26830), CYP71B38 (AT3G44250), CYP71A26 (AT3G48270), CYP71A25 (AT3G48280), CYP71A24 (AT3G48290), CYP71A22 (AT3G48310), CYP71A21 (AT3G48320), CYP71B5 (AT3G53280), CYP71B31 (AT3G53300), CYP71B32 (AT3G53305), CYP71A19(AT4G13290), CYP71A20 (AT4G13310), CYP71B11 (AT5G25120), CYP71B12(AT5G25130), CYP71B13 (AT5G25140), CYP71B14 (AT5G25180), CYP71B8 (AT5G35715), and CYP71B10 (AT5G57260). The iTOL (https://itol.embl.de/) was used to annotate the phylogenetic tree.

Statistical analysis

Results are expressed as means ± SD or ±SE as indicated in the figure legends and represent at least 3 biological repetitions. Statistical analysis was performed using Student's *t*-test. $P < 0.05$ was considered significant.

Accession numbers

Sequence data from this article can be found in the *Arabidopsis* Genome Initiative or GenBank/EMBL database under the following

accession numbers: *Arabidopsis*: *CYP71B3* (AT3G26220), *CYP71B22* (AT3G26200), *CYP71B20* (AT3G26180), *RTP1* (AT1G70260), *CYP71A13* (AT2G30770), *CYP71A12* (AT1G09080), *bZIP60* (AT1G42990), and *CYP71B15* (AT3G26830).

Acknowledgments

We thank Dr Karl-Heinz Kogel and Dr Patrick Schäfer (University of Giessen, Germany) for critical reading of the manuscript and Dr Yin Song (Northwest A&F University, China) and Guangyao Li (Peking University, China) for discussions and their insightful suggestions. We also thank Dr Fei Zhang and Dr Jing Zhang in Horticultural Science Research Center, Life Science Research Core Services, and Bioinformatic Platform of State Key Laboratory for Crop Stress Resistance and High-Efficiency Production (Northwest A&F University, China), for their excellent technical support and Dr. Mingxun Chen (Northwest A&F University, China) for providing PGreenII 62-SK and PGreenII 0800-LUC vectors.

Author contributions

X.Q. and W.S. conceived and designed the research. Y.W., D.Z., X.Q., Y.T., L.K., X.G., X.W., Y.Z., and Y.Y. performed the experiments. Y.W., D.Z., and X.Q. analyzed the data. X.Q. and Y.W. wrote the article with help of all authors.

Supplementary data

The following materials are available in the online version of this article.

Supplementary Figure S1. The DEGs in Arabidopsis rtp1 roots upon early infection by *P. parasitica*.

Supplementary Figure S2. The expression of CYP71B21 in *P. parasitica*-infected WT Col-0 and *rtp1* mutant plants.

Supplementary Figure S3. Analysis of the immune function of CYP71B3, CYP71B20, and CYP71B22 via Agrobacterium-mediated transient expression in leaves of *N. benthamiana*.

Supplementary Figure S4. The expression levels of CYP71B3 under flg22 treatment, biotic stresses, or abiotic stresses.

Supplementary Figure S5. CYP71B3 contributes to alleviate RTP1-mediated plant susceptibility to *P. parasitica*.

Supplementary Figure S6. The identification and seeding growth phenotype of Col-0, CYP71B3-CM, CYP71B3$^{(I38A)}$-CM, CYP71B3-OE, cyp71b3, and rtp1cyp71b3 plants.

Supplementary Figure S7. CYP71B3 plays a positive role in Arabidopsis resistance to *P. parasitica*, and its I-38 residue is vital for resistance function.

Supplementary Figure S8. Analyses on the expression of GFP-CYP71B3 and CYP71B3$^{\Delta AA29\text{-}AA45}$-mCherry proteins.

Supplementary Figure S9. The firefly LCI assay between RTP1 and CYP71B3, CYP71B3(I38A), or CYP71B3$^{\Delta AA29\text{-}AA45}$.

Supplementary Figure S10. Co-IP assays showing RTP1 interaction with CYP71B3.

Supplementary Figure S11. Protein stability of CYP71B3, coexpressed with RTP1 or FLAG-GFP, as analyzed by immunoblotting (IB).

Supplementary Figure S12. Phylogenetic tree of CYP71 family proteins and interactions between RTP1 and CYP71 family proteins upregulated in *P. parasitica*-infected *Arabidopsis rtp1* roots.

Supplementary Figure S13. Protein tertiary structures of CYP71B22.

Supplementary Figure S14. Protein tertiary structures of RTP1 and CYP71B3 and the protein docking between RTP1 and CYP71B3.

Supplementary Figure S15. Protein stability of CYP71B3$^{(I38A)}$, coexpressed with RTP1 or FLAG-GFP, as analyzed by immunoblotting (IB).

Supplementary Figure S16. Examination of purified recombinant proteins His-sumo-CYP71B3 and His-sumo-CYP71B3$^{(I38A)}$ by SDS–PAGE.

Supplementary Figure S17. CYP71B3 positively regulates the expression of flg22-responsive immune-related genes upon infection by *P. parasitica*.

Supplementary Figure S18. Structural visualization of the enzyme activity pocket of CYP71B3.

Supplementary Figure S19. Phylogenetic analysis of Arabidopsis cytochrome P450 (CYPs) and CYP71B3 homologous proteins.

Supplementary Figure S20. Quantitation of camalexin in *P. parasitica*-infected *Arabidopsis* Col-0 and *cyp71b3* plants.

Supplementary Figure S21. The expression levels of BIP3 and bZIP28 in *P. parasitica*-infected WT Col-0 and *cyp71b3* mutant plants.

Supplementary Table S1. RNA-Seq data of *CYP71* family genes (FPKM > 0).

Supplementary Table S2. The primers sequences used in this study.

Supplementary Methods S1. Camalexin quantification.

Supplementary Methods S2. Bioinformatic analysis tools.

Funding

This work was funded by National Natural Science Foundation of China (#31872657), National Key R&D Program of China (#2017YFD0200602-2), China Agriculture Research System (#CARS-09), and the State Administration of Foreign Experts Affairs (#B18042).

Conflict of interest statement. None declared.

Data availability

The data that support the findings of this study are available from the corresponding author upon reasonable request.

References

Ascencio-Ibáñez JT, Sozzani R, Lee T, Chu T, Wolfinger R, Cella R, Hanley-Bowdoin L. Global analysis of *Arabidopsis* gene expression uncovers a complex array of changes impacting pathogen response and cell cycle during geminivirus infection. *Plant Physiol.* 2008:148(1):436–454. https://doi.org/10.1104/pp.108.121038

Birkenbihl RP, Kracher B, Roccaro M, Somssich IE. Induced genome-wide binding of three *Arabidopsis* WRKY transcription factors during early MAMP-triggered immunity. *Plant Cell.* 2017:29(1):20–38. https://doi.org/10.1105/tpc.16.00681

Bolger AM, Marc L, Bjoern U. Trimmomatic: a flexible trimmer for Illumina sequence data. *Bioinformatics*. 2014:30(15):2114–2120. https://doi.org/10.1093/bioinformatics/btu170

Boller T, He SY. Innate immunity in plants: an arms race between pattern recognition receptors in plants and effectors in microbial pathogens. *Science*. 2009:324(5928):742–744. https://doi.org/10.1126/science.1171647

Chae HJ, Ke N, Kim HR, Chen S, Godzik A, Dickman M, Reed JC. Evolutionarily conserved cytoprotection provided by Bax Inhibitor-1 homologs from animals, plants, and yeast. *Gene*. 2003:323:101–113. https://doi.org/10.1016/j.gene.2003.09.011

Chen H, Yan Z, Shang Y, Lin H, Zhou JM. Firefly luciferase complementation imaging assay for protein-protein interactions in

plants. *Plant Physiol.* 2008:146(2):368–376. https://doi.org/10.1104/pp.107.111740

Dodds PN, Rathjen JP. Plant immunity: towards an integrated view of plant-pathogen interactions. *Nat Rev Genet.* 2010:11(8):539–548. https://doi.org/10.1038/nrg2812

Eulgem T, Rushton PJ, Robatzek S, Somssich IE. The WRKY superfamily of plant transcription factors. *Trends Plant Sci.* 2000:5(5):199–206. https://doi.org/10.1016/S1360-1385(00)01600-9

Fry W. *Phytophthora infestans*: the plant (and R gene) destroyer. *Mol Plant Pathol.* 2008:9(3):385–402. https://doi.org/10.1111/j.1364-3703.2007.00465.x

Glawischnig E. The role of cytochrome P450 enzymes in the biosynthesis of camalexin. *Biochem Soc Trans.* 2006:34(6):1206–1208. https://doi.org/10.1042/BST0341206

Gleave AP. A versatile binary vector system with a T-DNA organisational structure conducive to efficient integration of cloned DNA into the plant genome. *Plant Mol Biol.* 1992:20(6):1203–1207. https://doi.org/10.1007/BF00028910

Gómez-Gómez L, Boller T. FLS2: a LRR receptor-like kinase involved in recognition of the flagellin elicitor in *Arabidopsis*. *Mol Cell.* 2000:5(6):1003–1011. https://doi.org/10.1016/S1097-2765(00)80265-8

Jakoby M, Weisshaar B, Droge-Laser W, Vicente-Carbajosa J, Tiedemann J, Kroj T, Parcy F. bZIP transcription factors in *Arabidopsis*. *Trends Plant Sci.* 2002:7(3):106–111. https://doi.org/10.1016/S1360-1385(01)02223-3

Jones J, Dangl JL. The plant immune system. *Nature.* 2006:444(7117):323–329. https://doi.org/10.1038/nature05286

Kamoun S, Furzer O, Jones JDG, Judelson HS, Ali GS, Dalio RJD, Roy SG, Schena L, Zambounis A, Panabières F, *et al.* The Top 10 oomycete pathogens in molecular plant pathology. *Mol Plant Pathol.* 2015:16(4):413–434. https://doi.org/10.1111/mpp.12190

Kim D, Paggi JM, Park C, Bennett C, SL S. Graph-based genome alignment and genotyping with HISAT2 and HISAT-genotype. *Nat Biotechnol.* 2019:37(8):907–915. https://doi.org/10.1038/s41587-019-0201-4

Kliebenstein DJ, Rowe HC, Denby KJ. Secondary metabolites influence *Arabidopsis/Botrytis* interactions: variation in host production and pathogen sensitivity. *Plant J.* 2005:44(1):25–36. https://doi.org/10.1111/j.1365-313X.2005.02508.x

Kreps JA, Wu Y, Chang HS. Transcriptome changes for *Arabidopsis* in response to salt, osmotic, and cold stress. *Plant Physiol.* 2002:130(4):2129–2141. https://doi.org/10.1104/pp.008532

Li H, Handsaker B, Wysoker A, Fennell T, Ruan J, Homer N, Marth G, Abecasis G, Durbin R, Proc GPD. The sequence alignment/map format and SAMtools. *Bioinformatics.* 2009:25(16):2078–2079. https://doi.org/10.1093/bioinformatics/btp352

Li J, Deng F, Wang H, Qiang X, Meng Y, Shan W. The Raf-like kinase Raf36 negatively regulates plant resistance against the oomycete pathogen *Phytophthora parasitica* by targeting MKK2. *Mol Plant Pathol.* 2022:23(4):530–542. https://doi.org/10.1111/mpp.13176

Li T, Wang Q, Feng R, Li L, Ding L, Fan G, Li W, Du Y, Zhang M, Shan W, *et al.* Negative regulators of plant immunity derived from cinnamyl alcohol dehydrogenases are targeted by multiple *Phytophthora* Avr3a-like effectors. *New Phytol.* 2019. https://doi.org/10.1111/nph.16139

Liao Y, Smyth GK, Shi W. FeatureCounts: an efficient general purpose program for assigning sequence reads to genomic features. *Bioinformatics.* 2014:30(7):923. https://doi.org/10.1093/bioinformatics/btt656

Liu S, Kracher B, Ziegler J, Birkenbihl RP, Somssich IE. Negative regulation of ABA signaling by WRKY33 is critical for *Arabidopsis* immunity towards *Botrytis cinerea*. *Elife.* 2015:4:e07295. https://doi.org/10.7554/eLife.07295

Love MI, Huber W, Anders S. Moderated estimation of fold change and dispersion for RNA-seq data with DESeq2. *Genome Biol.* 2014:15(12). https://doi.org/10.1186/s13059-014-0550-8

Lu W, Deng F, Jia J, Chen X, Li J, Wen Q, Li T, Meng Y, Shan W. The *Arabidopsis thaliana* gene AtERF019 negatively regulates plant resistance to *Phytophthora parasitica* by suppressing PAMP-triggered immunity. *Mol Plant Pathol.* 2020:21(9):1179–1193. https://doi.org/10.1111/mpp.12971

Mao G, Meng X, Liu Y, Zheng Z, Chen Z, Zhang S. Phosphorylation of a WRKY transcription factor by two pathogen-responsive MAPKs drives phytoalexin biosynthesis in Arabidopsis. *Plant Cell.* 2011:23(4):1639–1653. https://doi.org/10.1105/tpc.111.084996

Meng Y, Huang Y, Wang Q, Wen Q, Jia J, Zhang Q, Huang G, Quan J, Shan W. Phenotypic and genetic characterization of resistance in *Arabidopsis thaliana* to the oomycete pathogen *Phytophthora parasitica*. *Front Plant Sci.* 2015:6:378. https://doi.org/10.3389/fpls.2015.00378

Meng Y, Zhang Q, Ding W, Shan W. *Phytophthora parasitica* : a model oomycete plant pathogen. *Mycology.* 2014:5(2):43–51. https://doi.org/10.1080/21501203.2014.917734

Mucha S, Heinzlmeir S, Kriechbaumer V, Strickland B, Glawischnig E. The formation of a camalexin biosynthetic metabolon. *Plant Cell.* 2019:31(11):2697–2710. https://doi.org/10.1105/tpc.19.00403

Müller TM, Böttcher C, Morbitzer R, Götz CC, Lehmann J, Lahaye T, Glawischnig E. TALEN-mediated generation and metabolic analysis of camalexin-deficient *cyp71a12cyp71a13* double knockout lines. *Plant Physiol.* 2015:168(3):849–858. https://doi.org/10.1104/pp.15.00481

Narusaka M, Shiraishi T, Iwabuchi M, Narusaka Y. The floral inoculating protocol: a simplified Arabidopsis thaliana transformation method modified from floral dipping. *Plant Biotechnology.* 2010:27(4):349–351. https://doi.org/10.5511/plantbiotechnology.27.349

Neve EPA, Ingelman-Sundberg M. Cytochrome P450 proteins: retention and distribution from the endoplasmic reticulum. *Curr Opin Drug Discov Devel.* 2010:13:78–85. https://10.1016/j.cct.2009.10.001

Pan Q, Cui B, Deng F, Quan J, Gary JL, Shan W. RTP1 encodes a novel endoplasmic reticulum (ER)-localized protein in *Arabidopsis* and negatively regulates resistance against biotrophic pathogens. *New Phytol.* 2016:209(4):1641–1654. https://doi.org/10.1111/nph.13707

Panstruga R, Dodds PN. Terrific protein traffic: the mystery of effector protein delivery by filamentous plant pathogens. *Science.* 2009:324(5928):748–750. https://doi.org/10.1126/science.1171652

Pavan S, Jacobsen E, Visser R, Bai Y. Loss of susceptibility as a novel breeding strategy for durable and broad-spectrum resistance. *Mol Breed.* 2010:25(1):1–12. https://doi.org/10.1007/s11032-009-9323-6

Petersen K, Fiil BK, Mundy J, Morten P. Downstream targets of WRKY33. *Plant Signal Behav.* 2008:3(11):1033–1034. https://doi.org/10.4161/psb.6878

Qiang X, Liu X, Wang X, Qing Z, Kang L, Gao X, Wei Y, Wu W, Zhao H, Shan W. Susceptibility factor RTP1 negatively regulates *Phytophthora parasitica* resistance via modulating UPR regulators bZIP60 and bZIP28. *Plant Physiol.* 2021:186(2):1269–1287. https://doi.org/10.1093/plphys/kiab126

Qiu JL, Fiil BK, Petersen K, Nielsen HB, Botanga CJ, Thorgrimsen S, Palma K, Suarez-Rodriguez MC, Sandbech-Clausen S, Lichota J, *et al.* *Arabidopsis* MAP kinase 4 regulates gene expression through transcription factor release in the nucleus. *EMBO J.* 2008:27(16):2214–2221. https://doi.org/10.1038/emboj.2008.147

Rallapalli G, Kemen EM, Robert-Seilaniantz A, Segonzac C, Etherington GJ, Sohn KH, MacLean D, Jones JDG. EXPRSS: an

Illumina based high-throughput expression-profiling method to reveal transcriptional dynamics. *BMC Genomics*. 2014:15(1):341. https://doi.org/10.1186/1471-2164-15-341

Schie CV, Takken F. Susceptibility Genes 101: How to Be a Good Host. *Annu Rev Phytopathol*. 2014:52(1):551–581. https://doi.org/10.1146/annurev-phyto-102313-045854

Schlaeppi K, Abou-Mansour E, Buchala A, Mauch F. Disease resistance of *Arabidopsis* to *Phytophthora brassicae* is established by the sequential action of indole glucosinolates and camalexin. *Plant J*. 2010:62(5):840–851. https://doi.org/10.1111/j.1365-313X.2010.04197.x

Schneider CA, Rasband WS, Eliceiri KW. Image to ImageJ: 25 years of image analysis. *Nat Methods*. 2012:9(7):671–675. https://doi.org/10.1038/nmeth.2089

Scholz SS, Schmidt-Heck W, Guthke R, Furch ACU, Reichelt M, Gershenzon J, Oelmüller R. *Verticillium dahliae-Arabidopsis* interaction causes changes in gene expression profiles and jasmonate levels on different time scales. *Front Microbiol*. 2018:9:217. https://doi.org/10.3389/fmicb.2018.00217

Sun L, Yang Z, Song Z, Wang M, Sun L, Lu S, Liu J. The plant-specific transcription factor gene *NAC103* is induced by bZIP60 through a new cis-regulatory element to modulate the unfolded protein response in *Arabidopsis*. *Plant J*. 2013:76(2):274–286. https://doi.org/10.1111/tpj.12287

Wang N, Tang C, Fan X, He M, Gan P, Zhang S, Hu Z, Wang X, Yan T, Shu W, *et al*. Inactivation of a wheat protein kinase gene confers broad spectrum resistance to rust fungi. *Cell*. 2022:185(16):2961–2974. https://doi.org/10.1016/j.cell.2022.06.027

Wang Y, Meng Y, Zhang M, Tong X, Wang Q, Sun Y, Quan J, Gover F, Shan W. Infection of *Arabidopsis thaliana* by *Phytophthora parasitica* and identification of variation in host specificity. *Mol Plant Pathol*. 2011:12(2):187–201. https://doi.org/10.1111/j.1364-3703.2010.00659.x

Wang Z, Gerstein M, Snyder M. RNA-Seq: a revolutionary tool for transcriptomics. *Nat Rev Genet*. 2009:10(1):57–63. https://doi.org/10.1038/nrg2484

Win J, Kamoun S, Jones AME. Purification of effector–target protein complexes via transient expression in *Nicotiana benthamiana*. *Methods in Molecular Biology*. 2011:712:181–194. https://doi.org/10.1007/978-1-61737-998-7_15

Wojtaszek P. Mechanisms for the generation of reactive oxygen species in plant defence response. *Acta Physiologiae Plantarum*. 1997:19(4):581–589. https://doi.org/10.1007/s11738-997-0057-y

Xu Q, Reed JC. Bax inhibitor-1, a mammalian apoptosis suppressor identified by functional screening in yeast. *Mol Cell*. 1998:1(3):337–346. https://doi.org/10.1016/S1097-2765(00)80034-9

Yang L, Zhang Y, Guan R, Li S, Xu X, Zhang S, Xu J. Co-regulation of indole glucosinolates and camalexin biosynthesis by CPK5/CPK6 and MPK3/MPK6 signaling pathways. *J Integr Plant Biol*. 2020a:62(11):142–158. https://doi.org/10.1111/jipb.12973

Yang Y, Fan G, Zhao Y, Wen Q, Peng W, Meng Y, Shan W. Cytidine-to-uridine RNA editing factor NBMORF8 negatively regulates plant immunity to *Phytophthora* pathogens. *Plant Physiol*. 2020b:184(4):2182–2198. https://doi.org/10.1104/pp.20.00458

Yang Y, Zhao Y, Zhang Y, Niu L, Li W, Lu W, Li J, Schafer P, Meng Y, Shan W. A mitochondrial RNA processing protein mediates plant immunity to a broad spectrum of pathogens by modulating the mitochondrial oxidative burst. *Plant Cell*. 2022:34(6):2343–2363. 10.1093/plcell/koac082.

Yoshihiro N, Mari N, Motoaki S, Junko I, Maiko N, Asako K, Akiko E, Tetsuya S, Masakazu S, Masatomo K. The cDNA microarray analysis using an Arabidopsis pad3 mutant reveals the expression profiles and classification of genes induced by *Alternaria brassicicola* attack. *Plant Cell Physiol*. 2003:4:377–387. https://doi.org/10.1093/pcp/pcg050

Yuan M, Jiang Z, Bi G, Nomura K, Xin X. Pattern-recognition receptors are required for NLR-mediated plant immunity. *Nature*. 2021:592(7852):105–109. https://doi.org/10.1038/s41586-021-03316-6

Zhang F, Fang H, Wang M, He F, Tao H, Wang R, Long J, Wang J, Wang G, Ning Y. APIP5 functions as a transcription factor and an RNA-binding protein to modulate cell death and immunity in rice. *Nucleic Acids Res*. 2022:50(9):5064–5507. https://doi.org/10.1093/nar/gkac316

Zhang H, Zhang F, Yu Y, Feng L, Jia J, Liu B, Li B, Guo H, Zhai J. A comprehensive online database for exploring~20,000 public *Arabidopsis* RNA-Seq libraries. *Mol Plant*. 2020:13(9):1231–1233. https://doi.org/10.1016/j.molp.2020.08.001

Zhang X, Henriques R, Lin S, Niu Q, Chua N. *Agrobacterium*-mediated transformation of *Arabidopsis thaliana* using the floral dip method. *Nature Protocol*. 2006:1(2):641–646. https://doi.org/10.1038/nprot.2006.97

Zhao Y, Hull AK, Gupta NR, Goss KA, Alonso J, Ecker JR, Normanly J, Chory J, Celenza JL. Trp-dependent auxin biosynthesis in *Arabidopsis*: involvement of cytochrome P450s CYP79B2 and CYP79B3. *Genes Dev*. 2003:16(23):3100–3112. https://doi.org/10.1101/gad.1035402

Zhou J, Wang X, He Y, Sang T, Wang P, Dai S, Zhang S, Meng X. Differential phosphorylation of the transcription factor WRKY33 by the protein kinases CPK5/CPK6 and MPK3/MPK6 cooperatively regulates camalexin biosynthesis in Arabidopsis. *Plant Cell*. 2020:32(8):2621–2638. https://doi.org/10.1105/tpc.19.00971